Excited electronic potential-energy surfaces and transition moments for the H_3 system

Zhengwei Peng,* Sandor Kristyan,† and Aron Kuppermann
Arthur Amos Noyes Laboratory of Chemical Physics, Division of Chemistry and Chemical Engineering, California Institute of Technology, Pasadena, California 91125

James S. Wright
Ottawa-Carleton Chemistry Institute, Carleton University, Ottawa, Canada K1S 5B6
(Received 30 January 1995)

Four electronic states of H_3 have been studied using a multiple-reference double-excitation configuration-interaction method with an extensive basis set of 75 Gaussian-type atomic orbitals. A total of 1340 *ab initio* points were calculated over a wide range of H_3 molecular geometries. These four states include the ground state and the Rydberg $2s\,^2A_1'$ and $2p_z\,^2A_2''$ states, as well as the state that in equilateral triangular geometry is related to the ground state by a conical intersection. Electric-dipole transition moments were also obtained between these states. The results show that the atomic and diatomic energetic asymptotes are accurately described. The barriers, wells, and energy differences also show good agreement compared to literature values, where available. The potential energies of the ground state and the $2p_z\,^2A_2''$ Rydberg state display smooth and regular behavior and were fitted over the whole molecular geometries using a rotated Morse curve-cubic spline approach. The other two potential-energy surfaces reveal more complicated behaviors, such as avoided crossings, and will require a different fitting procedure to obtain global fitting. Finally, dynamical implications of these potential surfaces and electric-dipole transition moments are discussed.

PACS number(s): 31.10.+z

I. INTRODUCTION

The first step toward understanding not only the structure but also the dynamics of a molecular system is to generate the potential-energy surfaces of its electronic states. Furthermore, if physical or chemical processes involving multiple electronic states are of interest, the electronically nonadiabatic coupling matrix elements and the radiation-assisted coupling elements (such as the electric-dipole transition moment) between electronic states are also needed.

The potential-energy surface of the ground electronic state of H_3 has been calculated since the beginning of quantum chemistry [1–12]. The high-quality ground electronic state potential energies obtained by Liu [6] and by Siegbahn and Liu [7] (hereafter SL) were fitted by Truhlar and Horowitz [13] to give the SLTH surface, which incorporated some scaling to produce accurate diatomic limits and for many years provided a standard of accuracy for the field. The more recent double many-body expansion (DMBE) surface of Varandas *et al.* [14] provides another fit to the SL energy data. Although it has a larger rms error than that of the SLTH surface, the DMBE surface is believed to be more accurate at higher energies [13,14]. The quality of the SLTH surface has been reconfirmed and extended by two more recent studies [11,12]. These potential-energy surfaces offer a good starting point for the quantum scattering calculation [15–49] of the $H+H_2$ (and also its isotopes) reaction, which is the prototypical gas-phase atom-diatom chemical reaction $A+BC \rightarrow AB+C$.

For excited states of the H_3 system, the number of available *ab initio* calculations is sparse and of small scale, although these excited states are of considerable current interest [50–77]. A review of all work on excited state surfaces of H_3 up to 1976 is given in Truhlar and Wyatt's [78] work. Reviews on the Rydberg excited states of H_3 have been given in the recent publications of Herzberg [79], Watson [80], and Gellene and Porter [81]. Important early theoretical work on the excited states of H_3 includes the studies of Rydberg spectra of H_3 by King and Morokuma [82], Jungen [83], Martin [84], Kulander and Guest [85], Nager and Jungen [86], and Raynor and Herschbach [87], and the series on transition state spectroscopy by Polanyi and co-workers [88–90]. A thorough study of excited electronic potential-energy surfaces of H_3 was done by Roach and Kuntz using the semiempirical diatom-in-a-molecule (DIM) method [91]. More recent work on H_3 was done by Petsalakis, Theodorakopoulos, and Wright [92] (hereafter PTW) and also by Diercksen, Duch, and Karwowski [93]. In a recent Letter, the current authors have also reported a calculation of the lowest four electronic states with fixed bond angles of 60° [94]. It must be mentioned that the work of Porter, Stevens, and Karplus [5] is not only on the ground state H_3 but is also a classic early paper on the excited state.

*Present address: Biosym Technologies, Inc., 9685 Scranton Road, San Diego, CA 92121.
†Present address: Department of Chemistry and Biochemistry, University of Arkansas at Fayetteville, Fayetteville, AR 72701.

The full potential-energy surface of the first excited state of H_3 (not a Rydberg state) has been obtained using a functional extrapolation scheme of the DMBE method, along with the major terms of the electronically nonadiabatic coupling elements near the equilateral triangular configuration between this state and the ground state [14]. There have not been any direct calculations of the nonadiabatic coupling terms between any pair of H_3 potential-energy surfaces. Because the DMBE functional extrapolation is valid only in the close vicinity of the conical intersection (the equilateral triangular H_3 configuration), the potential-energy surface of the first excited state in regions far away from the conical intersection is believed not to be accurate [14]. So far, most of the quantum scattering calculations of the $H+H_2$ system have been carried out on the single ground electronic potential-energy surface [15–49]. The geometric phase [95–100] induced by the conical intersection between the ground and the first excited states of H_3 has been demonstrated to have a profound effect on the rovibrational eigenenergies supported by the upper state [101,102]. It is also found to be important for the reactive scattering on the ground state at energies above 2.2 eV [103,104]. Even in these studies [103,104] only one potential-energy surface (the ground state) is considered explicitly. But when the total energy approaches 2.75 eV [with respect to $H(1s)+H_2(X\,^1\Sigma_g^+)$], which is the lowest value of the first excited potential-energy surface [14], it is necessary to include both potential-energy surfaces explicitly in the scattering calculations. Therefore it is our first objective to calculate, using *ab initio* methods, potential energies of the first excited H_3 electronic state over a wide region of molecular geometries. The result will allow us to address the inaccuracy in the upper sheet of the DMBE surface and pave the way for future high-energy H_3 scattering calculations. It is worth noting that semiclassical trajectory surface hopping calculations [105] were carried out for H_3 employing the DMBE excited surface.

The $2p_z\,^2A_2''$ excited state is very special among the low-lying H_3 Rydberg states [79–81]. The electronic energy levels and correlation diagram of H_3 in an equilateral triangular molecular configuration with an internuclear distance of 1.64 bohrs is shown in Fig. 1. Since the molecular point group for an equilateral triangle is D_{3h}, all electronic states are labeled according to the symmetry representation of this point group, along with the labels of the united-atom limits [57,58]. From symmetry arguments, Herzberg and co-workers [57,58] have pointed out its decay mechanism as the rovibronic predissociation [106] into the ground repulsive state and the electric-dipole radiation [107] into the lower $2s\,^2A_1'$ Rydberg state. The lifetime this electric-dipole transition between $2p_z\,^2A_2''$ and $2s\,^2A_1'$ has been estimated to be about 90 μsec [62,92,94]. More recent experiments have found that spin-orbital couplings also contribute to the decay of the $2p_z\,^2A_2''$ excited state [76,77]. In order to understand the decay lifetime of the $2p_z\,^2A_2''$ state, the full potential-energy surfaces of those four low-lying electronic states and some electric-dipole transition moments are needed (see Fig. 1). Previous theoretical studies on the excited

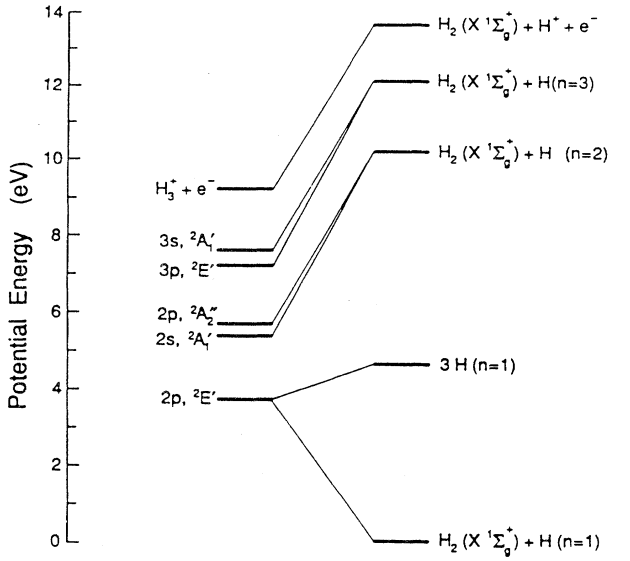

FIG. 1. Electronic energy level and correlation diagram of H_3. The spacing of the H_3 energy levels was calculated for an equilateral triangular configuration [82] with an internuclear distance of 1.64 bohrs and referred to the energy of dissociated products by the results of a separated calculation [85].

H_3 Rydberg states were more or less aimed at explaining the most obvious features of the experimental Rydberg spectroscopic results. The restricted molecular geometries in these studies for which *ab initio* calculations have been done prevented the construction of full potential-energy surfaces. In this sense, the theoretical study of the accurate rotational and vibrational structures of the H_3 Rydberg states is not possible for lack of full potential-energy surfaces, even though there is a great deal of experimental data available on this subject [57–61,66–77]. Therefore it is our second objective to calculate, using *ab initio* methods, potential energies of the H_3 excited $2p_z\,^2A_2''$ and $2s\,^2A_1'$ electronic states and the electric-dipole moment between each other over a wide region of molecular geometries.

Furthermore, transition-state spectroscopy [88–90, 108–116] and laser-assisted chemical reaction (laser catalysis) [117,118] have attracted a lot of attention recently. Both chemical processes involve at least two potential energy surfaces. For the H_3 system, the continuum radiation absorption spectrum between the ground electronic state and the third excited state (in D_{3h} nuclear geometry this corresponds to the $2p_z\,^2A_2''$ state) has been studied theoretically and the results have shown many phenomena that reveal rich and complex dynamics between these two potential-energy surfaces [112–116]. In these calculations, the SLTH surface is commonly used as the ground-state potential-energy surface and the semiempirical DIM surface developed by Mayne and co-workers as the $2p_z\,^2A_2''$ potential-energy surface [90]. The electric-dipole transition moment between the ground electronic state and the $2p_z\,^2A_2''$ excited state has been approximat-

ed by either a constant or a guessed switching function [88–90,115–118]. PTW [92] have compared their *ab initio* multiple-reference single- or double-excitation (MRSD) configuration-interaction (CI) results on H_3 with the extensive semiempirical DIM work by Roach and Kuntz [91] and found that the DIM calculations reproduced the gross features of the ground and excited potential surfaces but with some quantitative discrepancies [92]. We expect similar discrepancies to exist in the DIM potential surface of the $2p_z\,^2A_2''$ excited state by Mayne and co-workers [90]. Any improvement in the quality of the $2p_z\,^2A_2''$ excited potential-energy surface and its electric-dipole transition moment to the ground state will lead to a more realistic description of the chemical process involved and improve the comparison between theoretical and experimental results. Hence it is our third objective to calculate, using *ab initio* methods, potential energies of the $2p_z\,^2A_2''$ excited state and its electric-dipole transition moment to the ground state.

In this study, potential energies of the lowest four electronic states of H_3 ($2p_{xy}\,^2E'$, $2s\,^2A_1'$, and $2p_z\,^2A_2''$; see Fig. 1) have been calculated using an *ab initio* MRSD-CI method over a wide range of molecular geometries. Electric-dipole transition moments are also calculated between these states. Numerical details are presented in Sec. II. Results in some selected molecular geometries are tabulated and discussed in Sec. III. In Sec. IV we present the full three-dimensional fittings of the potential-energy surfaces for the ground state and the $2p_z\,^2A_2''$ excited states. A summary is given in Sec. V.

II. METHOD OF CALCULATION

The method of calculation and numerical details have been given in our previous publication [94]. The important points are reviewed here. There are two regions of H_3 molecular geometry of interest in our study: the Rydberg region, where three protons are fairly close to each other, and the atom-diatom region, where one H atom is far away from the diatomic molecule H_2. The lowest five states in the asymptotic region of $H+H_2$ correlate with the states [91]

$$H_2(X\,^1\Sigma_g^+)+H(1s)\,, \tag{1}$$

$$H_2(X\,^1\Sigma_g^+)+H(2s,2p_x,2p_y,2p_z)\,, \tag{2}$$

and

$$H_2(b\,^3\Sigma_u^+)+H(1s)\rightarrow 3H(1s)\,. \tag{3}$$

It is clear that our basis set should be able to describe the atomic $H(n=1,2)$ states [see Eqs. (1)–(3) and Fig. 1] and the lowest two diatomic states $H_2(X\,^1\Sigma_g^+)$ and $H_2(b\,^3\Sigma_u^+)$. So the choice of our basis set is determined by the necessity of obtaining the following: (i) accurate atomic excitation energies for $H(1s)\rightarrow H(2s)$ and $H(1s)\rightarrow H(2p)$ transitions, (ii) accurate values for the H_2 energy in its ground electronic state $H_2(X\,^1\Sigma_g^+)$ and excited state $H_2(b\,^3\Sigma_u^+)$, (iii) a ground-state surface for H_3 of accuracy comparable to that of the SLTH and DMBE surfaces [13,14], and (iv) reasonably good agreement with the observed Rydberg spectrum of H_3 and the recent calculations by PTW [92] and Diercksen [93].

After some experimentation, the basis sets used by Siegbahn and Liu [7] (for the ground state of H_3) and by Talbi and Saxon [119] (for the Rydberg spectrum of H_3^+) were adapted for the present purpose. The valence ($9s/4s$) contracted Gaussian-type orbital (GTO) basis functions are taken from LS [7], with an outer exponent 0.066 18. Three more Rydberg s-type GTO functions are added, with an approximately even-tempered ratio of 2.4, giving exponents 0.027 58, 0.011 49, and 0.004 20. The polarization and Rydberg p-type basis functions are taken from Talbi and Saxon [119], with exponents 1.6, 0.4, 0.09, and 0.025. Finally, the six-component d-type function with exponent 1.0 was taken from LS [7]. The final atomic basis set, denoted $12s4p1d/7s4p1d$, therefore has 25 contracted atomic orbitals (AOs), of which three s-type and two p-type functions are essentially Rydberg in nature. The parameters of the $12s4p1d/7s4p1d$ basis set are listed in Table I. In order to cover a wide range of molecular geometries and allow the proper dissociation, it was found necessary to place the full AO set on each atomic center, for a total basis set size of 75 AOs. Even with such a diffuse basis set, no linear dependence problems [119] were encountered as we used the HONDO routine [120] to evaluate necessary integrals.

The molecule was located in the xy plane with its geometry described by two bond lengths R_1 and R_2 and one bond angle γ (see Fig. 2). All calculations were carried out using the point group C_s, even though at some molecular geometries the symmetry of the molecule could be higher (C_{2v}, D_{3h}, etc.). In terms of the C_s point group, A'-type functions are symmetric with respect to the xy plane whereas A''-type functions are antisymmetric.

The self-consistent-field (SCF) molecular orbitals (MOs) were constructed using the occupation $(1a')^2(1a'')^1$, which is the dominant MO configuration

TABLE I. $12s4p1d/7s4p1d$ Gaussian-type basis set.

Orbital	i	ξ_i (a.u.)	C_i (a.u.)
$1s$	1	837.22	0.000 112
	2	123.524	0.000 895
	3	27.704 2	0.004 737
	4	7.825 99	0.019 518
	5	2.650 4	0.065 862
	6	0.938 258	0.178 008
$2s$	1	0.372 145	1.000 00
$3s$	1	0.155 838	1.000 00
$4s$	1	0.066 180	1.000 00
$5s$	1	0.027 580	1.000 00
$6s$	1	0.011 490	1.000 00
$7s$	1	0.004 200	1.000 00
$1p$	1	1.6	1.000 00
$2p$	1	0.40	1.000 00
$3p$	1	0.09	1.000 00
$4p$	1	0.025	1.000 00
$1d$	1	1.0	1.000 00

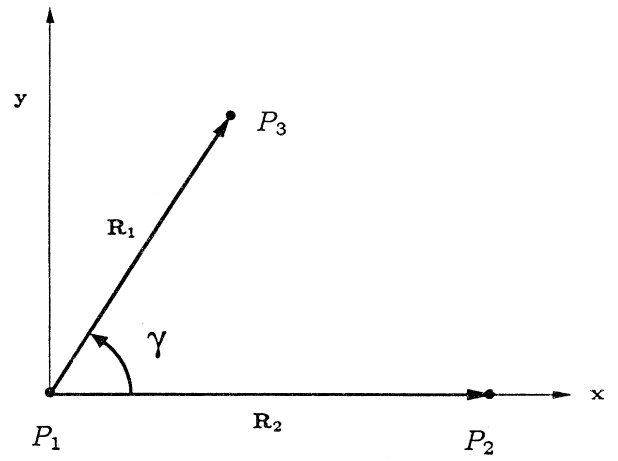

FIG. 2. Coordinate system used in the MRD-CI program. P_i is the ith proton of H_3. The three protons are all in the xy plane. The bond distance R_1 between P_1 and P_3, R_2 between P_1 and P_2, and the bond angle γ between them are used as the variables describing the shape of the triangle.

for the $2p_z\,^2A_2''$ electronic state when the molecule is near the equilateral triangular configuration and also for the $H(2p_z)+H_2(X\,^1\Sigma_g^+)$ state when the molecular geometry approaches the atom-diatom region. This choice of electron configuration will lead to SCF MOs that offer a very good description of the $2p_z\,^2A_2''$ state and also a more even-handed description of the two degenerate $2p_{xy}\,^2E'$ (the ground and first excited) electronic states near equilateral triangular configurations. The configuration-interaction energy is obtained using the MRD-CI method of Buenker and co-workers [121–127], with all 75 MOs kept in the calculation. The CI reference configuration space of A' symmetry was constructed using 45–49 reference configurations and the nature of these reference configurations depends on the molecular geometry. A configuration selection threshold energy of 2.0 μhartrees was chosen, which results in the generation of 50 000–60 000 configuration functions from which 4000–7000 were selected for the final CI calculation. For the lowest A_2''-type eigenvalue calculations, about 19–32 reference configurations were used. A threshold energy of 1.0 μhartrees results in 20 000–40 000 generated configurations, from which 600–3000 were selected. Extrapolation of the energy to zero threshold in the usual way gave the MRD-CI energy [121–125], which provided the raw data for constructing the potential-energy surfaces.

There are four electronic states of interest, whose energies we label as E_1, E_2, E_3, and E_4, where the first three are of A' symmetry and the last A'' symmetry. Using the symmetry notation appropriate for the equilateral triangular (D_{3h}) geometry, E_1 corresponds to the ground state $^2E'(1a'^2 1e')$, E_2 to the state degenerate with the ground one in the equilateral triangular geometry, E_3 to the $2s\,^2A_1'(1a'^2 2s)$ state, and E_4 to the $2p_z\,^2A_2''(1a'^2 2p_z)$ state. Although E_1 and E_2 are degenerate in the equilateral triangular geometry, such a degeneracy is lifted as soon as the triangle is distorted and this is what generates the conical intersection between the potential-energy surfaces of the E_1 and E_2 states [2,14]. We call the reader's attention to the notational difficulties: The notation E_i comes from the first letter of the word energy and is not an indication of state labels (since some of them have E symmetry only). We have chosen this notation again since it is compatible with our group's conventional notation used in other publications.

Electric-dipole transition moments between these states are also calculated at most molecular geometries. We label the moment between any two electronic states E_i and E_j as $\mathbf{T}_{ij}$. The C_s symmetry used in the calculation ensures that the electric-dipole transition moments between the antisymmetric E_4 state and the symmetric E_1, E_2, and E_3 states have only a z component and the transition moments among the symmetric states have no z component at all. Since the electron wave functions have been determined by the variational calculation to within a phase factor (real electronic wave functions can have a phase factor of $+1$ or -1 only), all electric-dipole transition moments are subject to an arbitrary sign change.

Selection of the geometries at which the *ab initio* calculations were done is guided by the rotated Morse curve spline (RMCS) potential-energy fitting method [128–130]. First, a bond angle γ is chosen and held fixed for the next series of calculations. A swing angle θ is defined as the angle by which the Morse curves are rotated with respect to the swing point P_s located at ($R_1^s=10$ bohrs, $R_2^s=10$ bohrs) in R_1 and R_2 Cartesian coordinates (see Fig. 3). The molecular geometry of a point

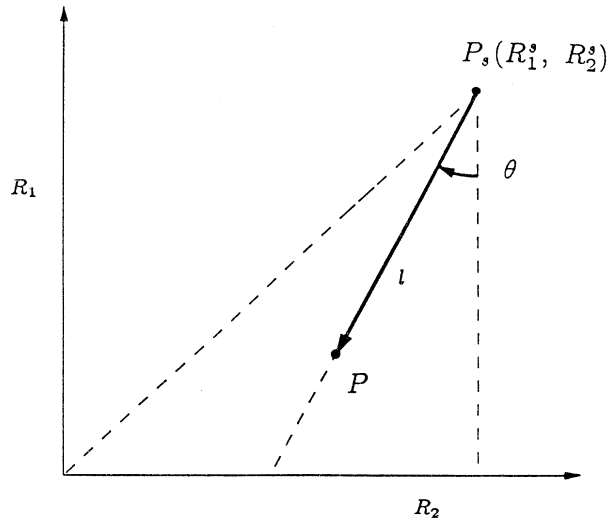

FIG. 3. Internal coordinate system used in the RMCS surface fitting scheme. In the R_1,R_2 Cartesian coordinates, P_s is the swing point with $R_1^s=R_2^s=10$ bohrs. A point P can be described by the swing angle θ and the swing distance l with respect to the swing point P_s.

along a ray with fixed (γ,θ) can be uniquely defined by its R_1 value. $\theta=0°$ corresponds to the ray with fixed $R_2=10$ bohrs and variable R_1 (atom-diatom region) and $\theta=45°$ corresponds to the symmetric $R_2=R_1$ configuration. Data points are taken at increments of 0.1–0.2 bohr from 1.0 to 3.0 bohrs in R_1. Typically 7–13 data points are calculated per ray (with a fixed γ and θ pair), while more points are added when necessary. A similar treatment was used by Mayne *et al.* [90], who interpolated DIM data using a rotated Morse curve approach.

Potential-energy data at each (γ,θ) ray were then fitted using a five-parameter generalized Morse function (GMF5) [131,132]

$$V=D_e\{(1.0-e^{\beta x})^2-1.0\}\ , \tag{4}$$

$$\beta=\beta_0(1+\lambda_1 x+\lambda_2 x^2)\ , \tag{5}$$

$$x=l-l_e\ , \tag{6}$$

with D_e the well depth relative to the swing point, l_e the distance of the minimum of the GMF5 function from the swing point, β_0 the curvature parameter, and λ_1 and λ_2 the linear and quadratic corrections to β_0, respectively. All five parameters are functions of γ and θ.

Ab initio calculations were performed for $\gamma=55°,60°,65°,75°,85°,90°,100°,110°,120°,150°,180°$ and $\theta=0°,20°,30°,35°,40°,41°,42°,43°,44°,45°$. The choice of γ comes from the fact that the permutation symmetry of H_3 allows us to use the largest bond angle ($\gamma_{\max}\geq 60°$) and the two bond lengths that form this γ angle to describe the H_3 molecular geometry. The permutation symmetry also allows us to reflect the calculated data with respect to $\theta=45°$ ($R_1\leftrightarrow R_2$) and therefore cover the full range of θ from 0° to 90° (see Fig. 3).

The major portion of the calculation has been done on the CRAY Y-MP machines of the NSF–San Diego Supercomputing Center and of the NAS program of the NASA–Ames Research Center and on the CRAY X-MP and Y-MP machines of the Jet Propulsion Laboratory. The CPU time on the CRAY Y-MP machines for a complete calculation at a single nuclear geometry took about 4–5 min for the symmetric potential energies (E_1,E_2,E_3) an additional 4–5 min for the antisymmetric potential energy (E_4), and about 1 min for the transition moments $(\mathbf{T}_{ij},\ 1\leq i,j\leq 4)$ reported. The intermediate files generated during a calculation can be as large as 38 megawords.

III. RESULTS AND DISCUSSION

A. Basis-set calibration

The quality of the AO basis set has been addressed in our previous paper [94]. Results for atomic and molecular hydrogen are given in Table II. The H(1*s*)→H(2*s*) transition energy is very accurate (10.2045 eV, which is within 0.0001 eV of the exact value), whereas the H(1*s*)→H(2*p*) transition energy is less accurate (10.2118 eV, an error of 0.0074 eV) due to fewer *p*-type Rydberg basis functions, but still quite good.

The energy of ground state $H_2(X\ ^1\Sigma_g^+)$ at internuclear distance of $R=1.4$ bohrs is close to that of Liu [6] and better than that of SL [7]. Combining the atomic and molecular energies, the computed energy well depth D_e is 4.7255 eV whereas the exact value is 4.7477 eV [133], an error of 0.02 eV. The excited state $H_2(b\ ^3\Sigma_u^+)$ is calculated to be 10.605 eV above the ground state, compared to the 10.623-eV value of Kolos and Wolniewicz [133]. So this important valence-shell transition is also accurately reproduced within 0.02 eV.

TABLE II. Selected results for the CI energy for H and H_2, using the $12s4p1d/7s4p1d$ basis set. Atomic energies are SCF orbital energies; molecular energies are full single- and double-excitation CI energies. R is the internuclear distance for H_2.

Species	R (bohrs)	Energy (hartrees)	Reference
H(1*s*)		−0.499 998	this work
H(1*s*)		−0.500 000	exact
H(2*s*)		−0.124 992	this work
H(2*s*)		−0.125 000	exact
H(2*p*)		−0.124 723	this work
H(2*p*)		−0.125 000	exact
$H_2(X\ ^1\Sigma_g^+)$	1.40	−1.173 652	this work
		−1.173 704	Liu [6]
		−1.173 3	SL [7]
		−1.174 474	KW [133]
$H_2(b\ ^3\Sigma_u^+)$	1.40	−0.783 904	this work
		−0.784 150	KW [133]

Tables III, IV, and V show the MRD-CI energies of the lowest four electronic states of H_3, for the equilateral triangular $(\gamma=60°,\theta=45°)$, symmetric collinear $(\gamma=180°,\theta=45°)$, and nonsymmetric collinear $(\gamma=180°,\theta=0°)$ molecular configurations, respectively.

The lowest-energy conical intersection for the E_1 state occurs at $R_1=R_2=R_3=1.9732$ bohrs, at an energy of −1.572 088 hartrees (GMF5 fit). The reference energy at the swing point P_s (Fig. 3) was chosen to be −1.499 994 hartrees, which is three times the calculated energy of an isolated H(1*s*) atom with our present basis set (see Table II). The reason for this choice instead of the theoretical value of −1.500 000 hartrees is for self-consistency. When fitting the E_3 surface, the reference energy at the swing point is chosen to be the SCF value of −1.124 988 hartrees (instead of −1.125 hartrees) for the separated H(2*s*)+H(1*s*)+H(1*s*) configuration. For E_4, the reference value at the swing point is chosen to be −1.124 718 hartrees for the separated $H(2p_z)+H(1s)+H(1s)$ configuration.

The minimum energy of E_1 with $\gamma=180°$ and $R_2=10$ bohrs occurs at $R_1=1.403$ bohrs, at an energy of =−1.673 022 hartrees (GMF5 fit). If we use this point to represent the $H(1s)+H_2(X\ ^1\Sigma_g^+)$ asymptotic state, then the lowest conical intersection point is 0.100 935 hartrees (2.747 eV) above the separated $H(1s)+H_2(X\ ^1\Sigma_g^+)$. For comparison, the corresponding energy for the SLTH surface [13] is 2.756 eV and occurs

TABLE III. Electronic potential energies (in hartrees) for equilateral triangular geometries. The origin of energy is that of the three electrons and the three protons at infinite separation. The energy of three separated H(1s) atoms is $-1.500\,000$ hartrees with respect to this origin. $R_1=R_2=R_3=R$. The state E_4 is antisymmetric with respect to the xy plane.

R (bohrs)	E_1	E_2	E_3	E_4
1.0	−1.286 448	−1.286 430	−1.280 663	−1.258 265
1.2	−1.441 703	−1.441 650	−1.415 028	−1.398 848
1.4	−1.518 046	−1.518 017	−1.468 988	−1.458 043
1.6	−1.554 349	−1.554 268	−1.482 113	−1.475 586
1.633	−1.557 748	−1.557 719	−1.481 972	−1.475 958
1.64	−1.558 556	−1.558 507	−1.481 895	−1.475 980
1.8	−1.569 022	−1.568 989	−1.474 258	−1.471 001
2.0	−1.571 945	−1.571 928	−1.455 205	−1.454 669
2.2	−1.568 548	−1.568 561	−1.430 550	−1.432 079
2.4	−1.561 349	−1.561 420	−1.403 023	−1.406 783
2.6	−1.552 813	−1.552 907	−1.375 206	−1.380 527
2.8	−1.544 312	−1.544 450	−1.347 990	−1.354 630
3.0	−1.536 907	−1.536 859	−1.322 044	−1.329 407

at $R_1=R_2=R_3=1.981$ bohrs. For the DMBE surface [14] the corresponding values are 2.749 eV and 1.973 bohrs. These results are listed in Table VI.

The saddle point in the collinear molecular configuration for the E_1 surface occurs at $R_1=R_2=(\frac{1}{2})R_3=1.758$ bohrs ($\gamma=180°, \theta=45°$) and at an energy of 0.440 eV (or 10.1 kcal/mole) (GMF5 fit) with respect to the energy of the separated $H+H_2(X\,^1\Sigma_g^+)$ (at $R_1=1.403$ bohrs, $R_2=10$ bohrs and $R_3=R_1+R_2=11.403$ bohrs, or the GMF5 fitted minimum point of E_1 along the cut $\gamma=180°$ and $\theta=0°$). We use this energy difference as the collinear barrier height of the $H+H_2$ reaction [7,13,14]. For comparison, the corresponding values for the SLTH surface [13] are 0.425 eV (or 9.80 kcal/mole) and 1.757 bohrs and for the DMBE surface [14] 0.418 eV (or 9.65 kcal/mole) and 1.755 bohrs. These results are listed in Table VII. As a result, the lowest-energy conical intersection and the corresponding geometry are in good agreement with accurate published values. For the saddle point in the collinear configuration, our calculated barrier height (which has not been scaled) and its location also agree well with the corresponding values of SLTH and DMBE surfaces.

The $E_1\rightarrow E_4$ transition energy for equilateral triangular configurations, corresponding to $e'\rightarrow 2p_z$, has been computed by Diercksen, Duch, and Karwowski [93] as

TABLE IV. Electronic potential energies (in hartrees) for symmetric linear geometries. The origin of energy is that of the six particles (three electrons and three protons) at infinite separation. The energy of three separated H(1s) atoms is $-1.500\,000$ hartrees with respect to this origin. $R_1=R_2=\frac{1}{2}R_3=R$. The state E_4 is antisymmetric with respect to the xy plane.

R (bohrs)	E_1	E_2	E_3	E_4
1.0	−1.434 609	−1.301 948	−1.283 374	−1.283 540
1.1	−1.510 762	−1.353 007	−1.336 663	−1.336 849
1.2	−1.564 466	−1.384 957	−1.370 293	−1.370 514
1.3	−1.601 646	−1.403 383	−1.390 318	−1.390 462
1.4	−1.626 915	−1.412 905	−1.400 325	−1.400 933
1.5	−1.643 011	−1.416 094	−1.403 978	−1.404 503
1.6	−1.652 252	−1.415 210	−1.402 812	−1.403 312
1.63	−1.653 734	−1.415 034	−1.401 517	−1.402 225
1.65	−1.654 444	−1.414 504	−1.400 590	−1.401 300
1.67	−1.655 162	−1.414 108	−1.399 519	−1.400 290
1.7	−1.656 114	−1.413 906	−1.398 229	−1.398 664
1.73	−1.656 952	−1.413 952	−1.396 053	−1.396 637
1.78	−1.656 513	−1.416 482	−1.392 451	−1.393 023
1.8	−1.656 594	−1.418 199	−1.391 131	−1.391 509
1.9	−1.653 957	−1.431 787	−1.385 831	−1.382 534
2.0	−1.649 371	−1.445 225	−1.377 716	−1.372 591
2.2	−1.636 000	−1.465 544	−1.358 956	−1.350 585

TABLE V. Electronic potential energies (in hartrees) for nonsymmetric linear geometries. The origin of energy is that of the six particles (three electrons and three protons) at infinite separation. The energy of three separated H(1s) atoms is $-1.500\,000$ hartrees with respect to this origin. The geometry is such that $R_1=R$, $R_2=10.0$ bohrs, and $R_3=R_1+R_2=R+10.0$ bohrs. The state E_4 is antisymmetric with respect to the xy plane.

R (bohrs)	E_1	E_2	E_3	E_4
1.0	−1.622 411	−1.247 049	−1.246 984	−1.247 192
1.1	−1.648 203	−1.273 168	−1.272 737	−1.272 967
1.2	−1.663 273	−1.287 824	−1.287 778	−1.288 010
1.3	−1.670 766	−1.295 032	−1.295 267	−1.295 499
1.4	−1.673 020	−1.297 355	−1.297 381	−1.297 734
1.5	−1.671 435	−1.309 302	−1.295 800	−1.296 085
1.6	−1.667 258	−1.331 377	−1.291 770	−1.291 910
1.7	−1.661 156	−1.350 706	−1.286 342	−1.285 818
1.8	−1.653 795	−1.367 858	−1.278 349	−1.278 448
1.9	−1.645 634	−1.383 097	−1.270 268	−1.270 237
2.0	−1.636 842	−1.396 687	−1.261 682	−1.261 512
2.1	−1.627 985	−1.408 843	−1.254 054	−1.252 511

well as by PTW [92]. Using $R_1=1.633$ bohrs and CI spaces of size 15 290, 22 570, and 47 060, Diercksen, Duch, and Karwowski obtained transition energies of 2.17, 2.21, and 2.11 eV, respectively. Our data at $R_1=1.633$ bohrs give 2.23 eV and PTW obtained 2.24 eV. From the experimental spectrum [80], we estimate that the vertical transition at $R_1=1.633$ bohrs should occur at about 2.15 eV, so that our present E_4 energy appears to be too high by about 0.08 eV. Possibly one more diffuse p function in the basis set would help to reduce this error. However, in general, our criteria for accurate multiple surface energetics have been met.

The squares $|\mathbf{T}_{ij}|^2$ of the electric-dipole transition moments between states E_i and E_j ($ij=21,31,32,43$) for equilateral triangular geometry (D_{3h}) are given in Table VIII. Allowed transitions in D_{3h} occur for $e'\rightarrow 2s$ ($\mathbf{T}_{31}$ and $\mathbf{T}_{32}$) and $2s\rightarrow 2p_z$($\mathbf{T}_{43}$). It can be seen that the $E_1\rightarrow E_2$ electric-dipole transition moment between two degenerate states is not zero since the calculation is carried out with the C_s symmetry and the description of the two states is not quite equivalent (see also Table III, where the E_1 and E_2 energies are not perfectly degenerate), but this transition moment is nevertheless small. $|\mathbf{T}_{43}|^2$ increases with R_1 and approaches its theoretical value of 9.00 a.u.^{2} when $R_1\rightarrow\infty$. Its value of 7.24 a.u.^{2} compares well with the PTW [92] value of 7.23 a.u.^{2} at $R_1=1.64$ bohrs. If the same method of estimation is used as by PTW [92], both results of $|\mathbf{T}_{43}|$ from PTW and our present work lead to the same lifetime of about 70 μsec for the $2p_z\,{}^2A_2''\rightarrow 2s\,{}^2A_1'$ electric-dipole radiative process [62,63]. In Table VIII, $|\mathbf{T}_{31}|^2$ and $|\mathbf{T}_{32}|^2$ are almost identical. They would be exactly identical if the D_{3h} symmetry instead of C_s had been used in the wave-function calculations. Their sum at 1.64 bohrs is 5.12 a.u.^{2}, while PTW [92] obtained 4.89 a.u.^{2}. One reason for the difference is that the present calculation employed a larger basis set. Another one is that in the current treatment we located Rydberg AOs on each atomic center, whereas PTW used a single Rydberg basis set located at the center of the triangle. The $|\mathbf{T}_{ij}|^2$ is the quantity that is related to experimental observables, e.g., absorption strength and oscillator strength. Figure 2 shows the (right-hand) orientation of the coordinate system for the values listed in Tables IX–XI.

TABLE VI. Lowest conical intersection energy and its corresponding geometry.

Property	E_1[a]	SLTH[b]	DMBE[c]
R[d]	1.973	1.981	1.973
E[e]	2.747	2.756	2.748

[a] E_1 is our *ab initio* data.
[b] See Ref. [13].
[c] See Ref. [14].
[d] $R_1=R_2=R_3=R$ in bohrs.
[e] The lowest conical intersection energy with respect to that of the separated H+H_2 configuration in eV. For the SLTH and DMBE surfaces, the accurate H+H_2 energy is used as the reference. For the present *ab initio* surface, the energy at the nuclear configuration with $R_1=1.402$ bohrs, $R_2=10$ bohrs, and $R_3=R_1+R_2=11.402$ bohrs is used instead. The difference between the second and the first of these reference energies is 0.040 eV.

In conclusion, the basis set we have used does satisfy all the selection criteria set previously. It gives good energy results of atomic H($n=1,2$) states, diatomic $H_2(X\,{}^1\Sigma_g^+)$ and $H_2(b\,{}^3\Sigma_u^+)$ states, and $n=1,2$ low-lying Rydberg states of H_3. It also gives good potential surface features of the ground state, which compared well with those of SLTH [13] and DMBE [14].

B. General features of the results

In this section, the general features of these four potential-energy surfaces and their transition moments are discussed in detail for some specific nuclear configurations.

TABLE VII. Saddle-point properties of the E_1 potential-energy surface.

Property	Liu[b]	SLTH[b]	DMBE[c]	RMCS[d]	*Ab initio*[e]
R_{SP} (bohrs)[a]	1.757	1.757	1.755	1.758	1.758
E_{SP} (eV)[a]	0.425	0.4251	0.418	0.440	0.443
k_s (eV/bohrs^2)[a]	2.90	2.93	2.95	2.90	2.90
k_a (eV/bohrs^2)[a]	−1.6	−1.57	−1.54	−1.46	

[a]The saddle-point geometry is described by $R_1=R_2=\frac{1}{2}R_3=R_{SP}$. E_{SP} is the barrier height of the saddle point. k_s is the force constant for the symmetric stretch mode defined by $g_s=\sqrt{3}/2(R_1+R_2-2R_{SP})$. k_a is the one for the asymmetric stretch mode defined by $g_a=\frac{1}{2}(R_1-R_2)$. E_1 is approximated with the diagonal form $\frac{1}{2}k_sg_s^2+\frac{1}{2}k_ag_a^2$ at the saddle point.

[b]See Ref. [13]. The barrier height is defined as the difference between the saddle-point energy and the accurate value [99] of the $H(1s)+H_2(X\,^1\Sigma_g^+)$ energy.

[c]See Ref. [14]. The barrier is defined in the same way as in footnote b.

[d]Present results for the E_1 RMCS surface. The barrier height is defined as the difference between the saddle-point energy and the energy at the nuclear configuration defined by $R_2=10$ bohrs and $R_1=1.402$ bohrs (at which value of R_1 for the given R_2 the present *ab initio* calculation has a minimum, as does the E_1 RMCS surface). The accurate Kolos-Wolniewicz [133] equilibrium internuclear distance is $R_1=1.401$ bohrs and has an energy 0.040 eV below the present one.

[e]The *ab initio* data are obtained from the results of the one-dimensional GMF5 fits. The definition of the barrier height is the same one defined in footnote d. The k_a value was not calculated for lack of a proper fit in the asymmetric mode to the *ab initio* data.

1. *Equilateral triangular configurations* (D_{3h})

More detailed studies of the *ab initio* results reveal some interesting points in the equilateral triangular nuclear configuration. Although C_s is the only symmetry embedded in the calculation, when three atomic centers form an equilateral triangle, the full molecular symmetry group D_{3h} will manifest itself via the following features.

(i) The two $2p_{xy}\,^2E'$ (E_1 and E_2) states are nearly degenerate.

(ii) The dipole transition moments $\mathbf{T}_{41}$ and $\mathbf{T}_{42}$ ($2p_z\,^2A_2''\rightarrow 2p_{xy}\,^2E'$) vanish due to symmetry reasons.

(iii) The $2p_{xy}\,^2E'$ states can always be rewritten as

$$|2p_x\,^2E'\rangle=\cos\phi|\varphi_1\rangle+\sin\phi|\varphi_2\rangle\ , \tag{7}$$

$$|2p_y\,^2E'\rangle=-\sin\phi|\varphi_1\rangle+\cos\phi|\varphi_2\rangle\ . \tag{8}$$

$|\varphi_1\rangle$ and $|\varphi_2\rangle$ are solutions of the electronic wave equation with the same energy, which form another E' representation of the D_{3h} group. The phase ϕ is not determined by the variational method and can have an arbitrary value. For two calculations with different internuclear distances, the relative phases of these two calculations are random, which in turn causes the x and y components of the transition moments $\mathbf{T}_{31}$, $\mathbf{T}_{32}$, and $\mathbf{T}_{21}$ to vary greatly (see Table IX). Even so, the D_{3h} symmetry ensures that the magnitudes of $\mathbf{T}_{31}$, $\mathbf{T}_{32}$, and $\mathbf{T}_{21}$ do not depend on the phase ϕ and thus should change smoothly with the internuclear distance and $|\mathbf{T}_{31}|=|\mathbf{T}_{32}|$, $|\mathbf{T}_{31}(x)|=|\mathbf{T}_{32}(y)|$, and $|\mathbf{T}_{31}(y)|=|\mathbf{T}_{32}(x)|$.

All these features are confirmed numerically by the results listed in Tables III and IX and by Figs. 4–6. Since the molecular properties are more sensitive to the quality of the wave functions than are the energy eigenvalues, the results of these transition moments offer another strong indication that the obtained wave functions are of good quality.

The results of the GMF5 fit show that E_1 has a barrier of 2.747 eV (relative to $H+H_2$) at $R=1.973$ bohrs. The surfaces E_3 and E_4 have a deep potential well of magnitude 9.721 and 9.558 eV, relative to their three-atom asymptote. These occur at $R=1.604$ bohrs for E_3 and $R=1.642$ bohrs for E_4, respectively. At $R=1.64$ bohrs, the *ab initio* energy spacing between states $2s\,^2A_1'$ and $2p\,^2A_2''$ is 1299 cm^{-1}, while the best value obtained by

TABLE VIII. Square of the absolute value of the electric-dipole transition moment $|\mathbf{T}_{ij}|^2$ (in units of a.u.^{2}) of H_3 for the equilateral triangular geometries. $\mathbf{T}_{ij}$ is the transition dipole vector between i and j states. The indices 1, 2, 3, and 4 refer to states E_1, E_2, E_3, and E_4, respectively.

R (bohrs)	$\lvert\mathbf{T}_{21}\rvert^2$	$\lvert\mathbf{T}_{31}\rvert^2$	$\lvert\mathbf{T}_{32}\rvert^2$	$\lvert\mathbf{T}_{43}\rvert^2$
1.0	0.004	5.07	5.18	6.81
1.2	0.009	4.20	4.20	6.92
1.4	0.018	3.38	3.42	7.02
1.6	0.030	2.70	2.68	7.18
1.633	0.032	2.59	2.60	7.22
1.64	0.033	2.54	2.58	7.24
1.8	0.047	2.12	2.12	7.34
2.0	0.061	1.70	1.70	7.51
2.2	0.071	1.32	1.30	7.56
2.4	0.077	1.07	1.05	7.73
2.6	0.073	0.858	0.860	7.84
2.8	0.063	0.689	0.612	7.90
3.0	0.049	0.559	0.548	7.95

TABLE IX. Absolute value of the component of the electric-dipole transition moment (in a.u.) between the four calculated electronic states for equilateral triangular geometries. $\mathbf{T}_{ij}$ is the transition dipole vector between i and j states. The indices 1, 2, 3, and 4 refer to states E_1, E_2, E_3, and E_4, respectively. 432[−3] means 0.432×10^{-3}. $R_1=R_2=R_3=R$.

R (bohrs)	$\lvert\mathbf{T}_{41}(z)\rvert$	$\lvert\mathbf{T}_{42}(z)\rvert$	$\lvert\mathbf{T}_{43}(z)\rvert$	$\lvert\mathbf{T}_{31}(x)\rvert$	$\lvert\mathbf{T}_{31}(y)\rvert$	$\lvert\mathbf{T}_{32}(x)\rvert$	$\lvert\mathbf{T}_{32}(y)\rvert$	$\lvert\mathbf{T}_{21}(x)\rvert$	$\lvert\mathbf{T}_{21}(y)\rvert$
1.0	0.432[−3]	0.194[−3]	2.61	2.25	0.944[−1]	0.927[−1]	2.26	0.586[−1]	0.521[−1]
1.2	0.541[−3]	0.120[−3]	2.63	0.199	2.04	2.04	0.198	0.916[−1]	0.182[−1]
1.4	0.483[−3]	0.489[−3]	2.65	0.161	1.83	1.84	0.159	0.131	0.227[−1]
1.6	0.809[−3]	0.546[−3]	2.68	1.22	1.10	1.09	1.22	0.202[−1]	0.172
1.633	0.557[−3]	0.922[−3]	2.69	1.21	1.06	1.06	1.21	0.235[−1]	0.179
1.64	0.830[−3]	0.378[−3]	2.69	1.38	0.801	0.803	1.39	0.909[−1]	0.157
1.8	0.647[−3]	0.538[−3]	2.71	0.362	1.41	1.41	0.361	0.189	0.103
2.0	0.497[−3]	0.732[−3]	2.74	0.372	1.25	1.25	0.371	0.207	0.135
2.2	0.140[−3]	0.100[−2]	2.75	0.424	1.07	1.06	0.421	0.194	0.182
2.4	0.904[−3]	0.556[−3]	2.78	0.474	0.918	0.917	0.472	0.161	0.225
2.6	0.152[−2]	0.153[−3]	2.80	0.446	0.812	0.814	0.444	0.148	0.226
2.8	0.150[−2]	0.206[−3]	2.81	0.443	0.702	0.700	0.439	0.111	0.226
3.0	0.710[−3]	0.758[−4]	2.82	0.388	0.639	0.632	0.385	0.104	0.196

PTW [92] is 1422 cm^{-1} and the experimental estimation of the energy difference between the minima of those two states [80,92] is 1256 cm^{-1}. Because $R=1.64$ bohrs is not the location of the real minimum of the E_3 potential curve, the estimations of energy differences between the $2s\,^2A_1'$ state and the $2p_z\,^2A_2''$ state at 1.64 bohrs is not appropriate to be compared with the experimental value. The bottom of the E_3 equilateral triangular curve is located at 1.604 bohrs and that of the corresponding E_4 curve is at 1.642 bohrs (GMF5 fit). These two values agree very well with the experimental values of 1.606 and 1.640 bohrs [80]. The energy difference between these two minima is 1374 cm^{-1}, which is still 100 cm^{-1} larger than the experimental value.

TABLE X. Absolute value of the Z component of the electric-dipole transition moment (in a.u.) from E_4 to E_1, E_2, and E_3 for symmetric collinear geometries. $\mathbf{T}_{ij}$ is the transition dipole vector between i and j states. The indices 1, 2, 3, and 4 refer to states E_1, E_2, E_3, and E_4, respectively. 0.432[−3] means 0.432×10^{-3}. $R_1=R_2=\frac{1}{2}R_3=R$.

R (bohrs)	$\lvert\mathbf{T}_{41}(z)\rvert$	$\lvert\mathbf{T}_{42}(z)\rvert$	$\lvert\mathbf{T}_{43}(z)\rvert$
1.0	0.130[−5]	2.68	0.656[−5]
1.1	0.227[−5]	2.69	0.505[−5]
1.2	0.853[−6]	2.68	0.361[−5]
1.3	0.675[−6]	2.69	0.464[−5]
1.4	0.278[−5]	2.68	0.160[−4]
1.5	0.517[−6]	2.65	0.175[−5]
1.6	0.202[−5]	2.57	0.548[−5]
1.63	0.143[−5]	2.47	0.157[−6]
1.65	0.227[−6]	2.43	0.300[−5]
1.67	0.357[−5]	2.37	0.134[−5]
1.7	0.151[−7]	2.22	0.199[−5]
1.73	0.402[−2]	2.00	0.139[−5]
1.78	0.120[−5]	1.46	0.708[−5]
1.8	0.558[−6]	1.24	0.142[−6]
1.9	0.195[−6]	0.513	2.68
2.0	0.137[−5]	0.260	2.66
2.2	0.111[−6]	0.879[−1]	2.49

2. *Collinear configurations* ($C_{\infty v}$)

The energies of E_1, E_2, E_3, and E_4 in symmetric collinear geometries ($R_1=R_2=\frac{1}{2}R_3$) are listed in Table IV. Figure 7 shows the good agreement between our present *ab initio* results and that of the lower sheet of the DMBE surface [14]. The bottoms of the curves for the DMBE surface and for our E_1 GMF5 fit are located at $R_1=R_2=\frac{1}{2}R_3=1.755$ and 1.758 bohrs, respectively, an almost perfect agreement. Even in this collinear symmetric stretch mode, the E_4 state still has a deep minimum of 7.6164 eV (with respect to its three-atom asymptote) at $R_1=R_2=\frac{1}{2}R_3=1.5189$ bohrs. Following

TABLE XI. Absolute value of the Z component of the electric-dipole transition moment (in a.u.) between E_4 and E_1, E_2, and E_3 for nonsymmetric collinear geometries. $\mathbf{T}_{ij}$ is the transition dipole vector between i and j states. The indices 1, 2, 3, and 4 refer to states E_1, E_2, E_3, and E_4, respectively. 0.432[−3] means 0.432×10^{-3}. $R_1=R$, $R_2=10.0$ bohrs, and $R_3=R_1+R_2$.

R (bohrs)	$\lvert\mathbf{T}_{41}(z)\rvert$	$\lvert\mathbf{T}_{42}(z)\rvert$	$\lvert\mathbf{T}_{43}(z)\rvert$
1.0	0.743	2.46	0.436[−6]
1.1	0.743	2.45	0.872[−6]
1.2	0.742	2.55	0.469[−7]
1.3	0.741	2.64	0.756[−8]
1.4	0.741	2.60	0.186[−6]
1.5	0.747	0.108	0.152[−2]
1.6	0.740	0.702[−3]	1.31
1.7	0.751	0.388[−3]	2.33
1.8	0.751	0.282[−3]	2.07
1.9	0.749	0.190[−3]	1.87
2.0	0.748	0.158[−3]	1.87
2.1	0.756	0.935[−3]	0.114

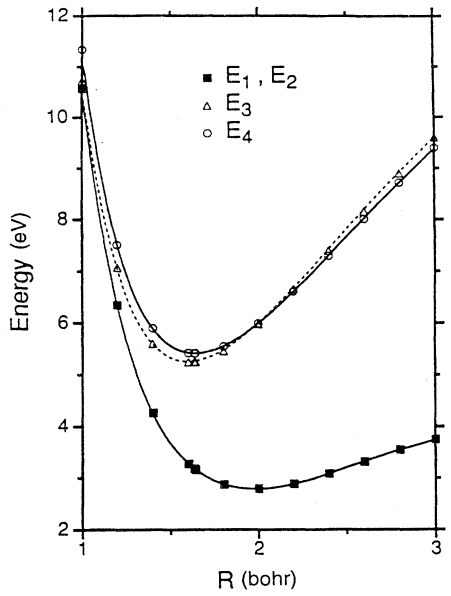

FIG. 4. Potential-energy curves for equilateral H_3. R is the length of the side of the triangle. In equilateral configurations, the E_1 and E_2 states are degenerate with each other. The energy origin is $-1.674\,474$ hartrees [$=(-0.5-1.174\,474)$ hartrees, the accurate $H(1s)+H_2(X\,^1\Sigma_g^+)$ value [133]], the same as that used in SLTH [13] and DMBE [14].

the $D_{\infty v}$ symmetry argument, the electric-dipole transition moment between the E_1 and E_4 states is supposed to be zero, as shown by our T_{41} results (see Table X). Since the upper sheet of the DMBE surface did not include the effect of avoided crossings of that state with other states, its behavior is quite different from our *ab initio* results

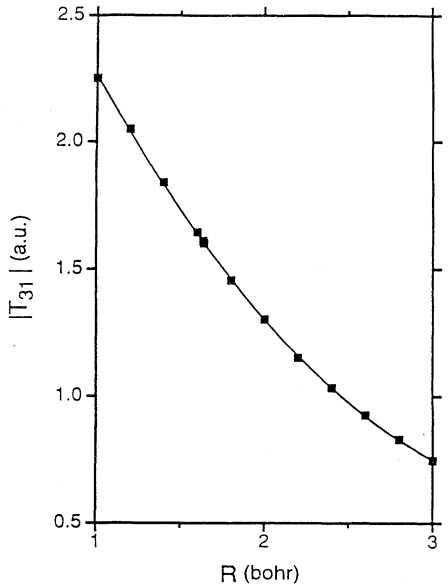

FIG. 5. Magnitude of the electric-dipole transition moment T_{31} between the E_3 and E_1 states for equilateral H_3. R is the length of the side of the triangle.

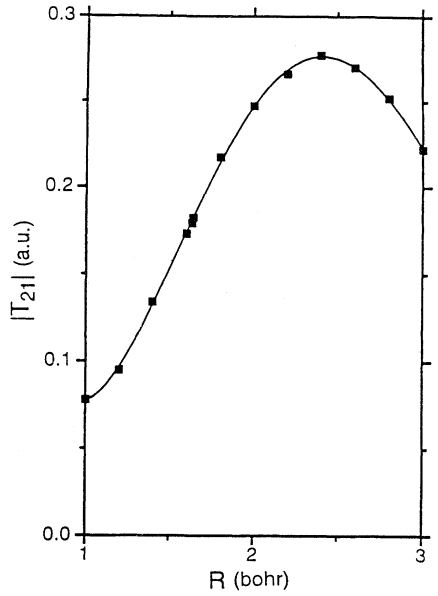

FIG. 6. Magnitude of the electric-dipole transition moment T_{21} between the E_2 and E_1 states for equilateral H_3. R is the length of the side of the triangle.

(see Fig. 8). The behavior of our results are in good agreement with those obtained by PTW [92] with an avoided crossing around $R_1=R_2=1.75$ bohrs. The effect of this avoided crossing is also demonstrated by the decrease of the transition moment $T_{42}(z)$ as R increases from 1.7 to 1.9 bohrs (see Table X). An even more abrupt change occurs in $T_{43}(z)$ around $R=1.9$ bohrs (see Table X). Further analysis shows that the wave function of the E_3 state when $R \leq 1.8$ bohrs is antisymmetric with respect to the plane formed by the z axis and the line that

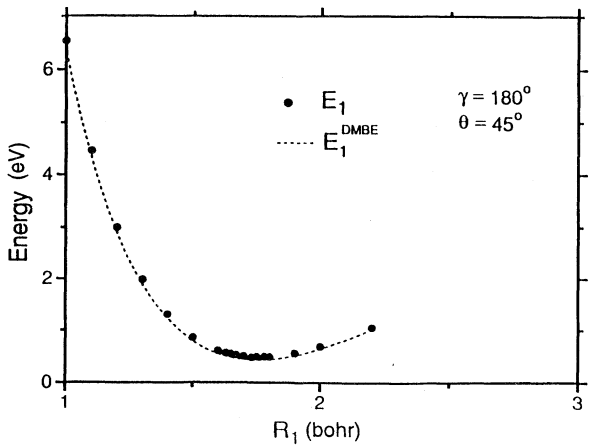

FIG. 7. Comparison between the DMBE ground potential-energy surface and the present E_1 *ab initio* results. The molecule is in a symmetric collinear configuration with $R_1=R_2=\frac{1}{2}R_3$, corresponding to $\gamma=180°$ and $\theta=45°$. The energy origin is that of Fig. 4.

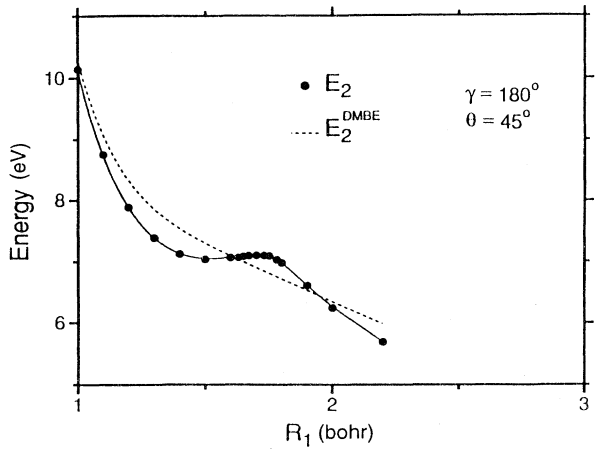

FIG. 8. Comparison between the upper sheet of the DMBE surface and the present E_2 *ab initio* results. See Fig. 7 for other details.

contains these three atomic centers. Then it becomes symmetric after $R \geq 1.9$ bohrs. This crossing is not avoided because of different symmetries the wave function has before and after. To some extent, the avoided crossing in E_2 induces the second crossing in E_3 since the former changes the energy ordering, which leads to new state assignment for E_3. If $C_{\infty v}$ is embedded into the calculation instead of C_s, the state assignment of E_3 will not be affected by the avoided crossing in E_2, which is of different symmetry, and $\mathbf{T}_{43}$ will have no abrupt changes at all. Here we leave the second crossing uncorrected because it serves as a reminder that when H_3 starts to bend, the second crossing will become a real avoided crossing.

In the nonsymmetric collinear configuration with $\gamma = 180°$ and $\theta = 0°$, which corresponds to the asymptotic $H + H_2$ situation, the potential curves of E_1 and E_4 are parallel to each other (see Table V), with almost the identical GMF5 Morse parameters. Both curves give well depths of 4.707 eV around $R_1 = 1.403$ bohrs. The corresponding accurate value for isolated $H_2(X\,^1\Sigma_g^+)$ from Kolos and Wolniewicz [133] is 4.7477 eV at a bond distance of 1.401 bohrs. Our full CI result for $H_2(X\,^1\Sigma_g^+)$ gives 4.7255 eV at a bond distance of 1.40 bohrs (Table II). These three sets of data agree with each other reasonably well. The electric-dipole transition moment $\mathbf{T}_{41}$ between these two states varies little with the diatomic bond distance and has a value between 0.74 and 0.75 a.u. (Table XI). For comparison, the electric-dipole transition moment of an isolated H atom from $1s \rightarrow 2p_z$ is 0.745 a.u. This excellent agreement suggests that our calculated E_1 and E_4 states are very close to the theoretical predictions of separated $H(1s,2p_z) + H_2(X\,^1\Sigma_g^+)$ states.

For a separated $H + H_2$ system, the repulsive potential-energy curve of $H(1s) + H_2(b\,^3\Sigma_u^+)$ intersects the curves of $H(2s,2p_x,2p_y,2p_z) + H_2(X\,^1\Sigma_g^+)$ around the diatomic bond distance of 1.45 bohrs. The potential-energy curves of $H(2s,2p_x,2p_y,2p_z) + H_2(X\,^1\Sigma_g^+)$ intersect the curve of $H(1s) + H_2(b\,^3\Sigma_u^+)$ around the diatomic bond distance of 2.2 bohrs [91]. For finite distance between H and H_2, many crossings are avoided. From our results along the ray of $\gamma = 180°$ and $\theta = 0°$ (see Table V and Fig. 9), the avoided crossing in E_2 around 1.4 bohrs can be seen clearly. Its potential energy curve has a sharp downward turn with increasing R_1. The electric-dipole transition moment $\mathbf{T}_{42}$ between the E_4 and E_2 states also has a sudden change in the same region (see Table XI). The calculated value of $|\mathbf{T}_{42}(z)|$ is around 2.5 a.u. before the crossing and drops below 0.002 a.u. after that, while the corresponding value for the $H(2s) \rightarrow H(2p_z)$ transition is 3.00 a.u. and the values for the $H(2p_{xy}) \rightarrow H(2p_z)$ transitions vanish by symmetry.

The potential-energy curve for the E_3 state is relatively smooth, although there are changes in $|\mathbf{T}_{43}(z)|$ for $R > 1.5$ bohrs. By analyzing the dominant coefficients of the MOs in the E_2 and E_3 CI wave functions (for $1.0 \leq R \leq 2.1$), we find five kinds of CI wave functions with unique patterns of dominant MO coefficients. Here we label them as S_1, S_2, S_3, S_4, and S_5. S_1 is associated with the asymptotic $H(2s) + H_2(X\,^1\Sigma_g^+)$ state, S_2 with $H(2p_{xy}) + H_2(X\,^1\Sigma_g^+)$ (with its p-orbital perpendicular to the plane formed by the z axis and the line containing three atomic center), S_3 with the repulsive $H(1s) + H_2(b\,^3\Sigma_u^+)$ state, and S_5 with $H(1s) + H_2(b\,^3\Sigma_u^+)$. The S_4 configuration has different characteristics, but we were not able to assign it to a known asymptotic state. The investigation of the E_1 and E_4 states also confirms that the E_1 state corresponds to the asymptotic $H(1s) + H_2(X\,^1\Sigma_g^+)$ state and E_4 corresponds to $H(2p_z) + H_2(X\,^1\Sigma_g^+)$. The electric-dipole transition moments between the S_1, S_2, S_3, S_4, and S_5 states and the E_4 state vary slowly as functions of R.

For $1.0 \leq R \leq 1.4$, E_2 is of the S_1 kind and E_3 the S_2 kind. This explains the smooth variations in the values of $|\mathbf{T}_{42}(z)|$ and $|\mathbf{T}_{43}(z)|$ (see Table XI). For $1.5 \leq R \leq 1.6$, E_2 undergoes an avoided crossing from the S_1 kind to the

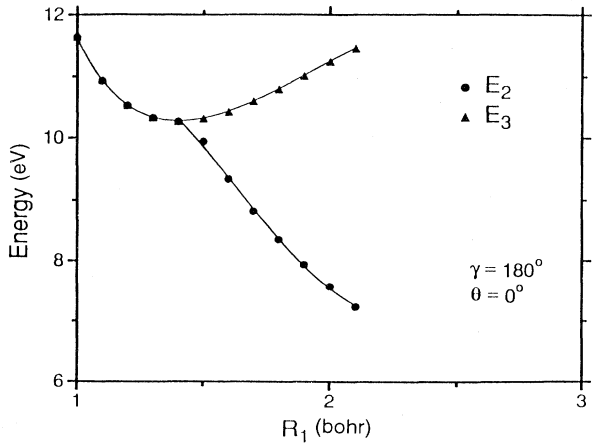

FIG. 9. Potential-energy curves for the E_2 and E_3 states for the nonsymmetric collinear geometry. The energy origin is that of Fig. 4.

S_3 kind and remains in S_3 afterward and E_3 switches into the S_4 kind (see Table XI). For $1.7 \leq R \leq 2.0$, E_3 becomes the S_1 kind with the right magnitude of T_{43}. At $R=2.1$, E_3 again switches from S_1 to S_5 with a sudden decrease in T_{43}.

As shown above, we have established a one-to-one correspondence between the changes in $|T_{42}(z)|$ and $|T_{43}(z)|$ and the variation in the nature of E_2 and E_3. Since all those asymptotic states are nearly degenerate with each other, even though there are many changes in the nature of E_3, the energy of E_3 still remains relatively smooth. We also find that S_1, S_3, S_4, and S_5 are symmetric with respect to the plane formed by the z axis and the line containing these three atomic centers and S_2 is antisymmetric. If $C_{\infty v}$ is used, E_3 would continue to be S_2 throughout the region $1.0 \leq R \leq 2.1$. Again we leave the state assignment of E_3 uncorrected to serve as a reminder that when H_3 starts to bend, all the crossings in E_3 will become avoided ones and the situation is going to be very complicated.

3. *General features of E_2 and E_3*

Because the number of *ab initio* calculations is large, we limit our scope to the bond angle $\gamma=60°$ for the discussion of general features of E_2 and E_3. For γ values of 55°, 65°, 75°, 85°, 90°, 100°, 110°, 120°, 150°, and 180°, the behavior is similar.

In the equilateral triangular geometry $\gamma=60°$ and $\theta=45°$, the E_2 state is degenerate with the ground state E_1 and has a shallow well at an internuclear distance of 1.973 bohrs (see Fig. 10). When θ decreases, the well depth also decreases and disappears at $\theta=42°$. After that, the curve becomes purely repulsive. When θ reaches 30°, one more feature appears around $R_1=1.5$ bohrs, signaling an avoided crossing. At this $\gamma=60°$, $\theta=30°$ cut of the E_2 potential-energy surface, the internuclear distances are not too large and the interaction between the two electronic states involved in the avoided crossing is strong. For this reason, the transition from one state to another is smooth over a wide range of nuclear geometries. When θ further decreases, the nuclear configuration approaches the separated $H+H_2$ asymptotic situation and the interaction between the two states involved in the avoided crossing becomes weaker. As a result, the transition from one state to another becomes more abrupt in a small region of nuclear geometries.

The behavior of E_3 is more complicated. In the range of $42° \leq \theta \leq 45°$, the E_3 potential-energy curve has a deep well, with a Morse-like behavior. At $\theta=41°$, a new feature appears around $R_1=2.4$ bohrs. This feature becomes more pronounced at $\theta=40°$ and the slope of the curve for large R_1 becomes small. When θ reaches 30°, the potential-energy curve does not have a well in the range $1.0 \leq R_1 \leq 2.0$ bohrs. At $\theta=20°$, there are again two features in the potential-energy curve with a transition point at $R_1=1.8$ bohrs. At $\theta=0°$, the potential-energy curve has a Morse shape up to $R_1=2.0$ bohrs. From the limited amount of *ab initio* data available, we are already able to see the significant complexity in the potential-energy surface of the E_3 state. We have attempted to understand what asymptotic states are involved in the fine surface features, but have not yet been able to accomplish this. Calculations involving higher-energy surfaces may be required for this purpose.

For $\gamma=55°$, 65°, 75°, 85°, 90°, 100°, 110°, 120°, 150°, and 180°, the main features of the E_2 and E_3 states are similar

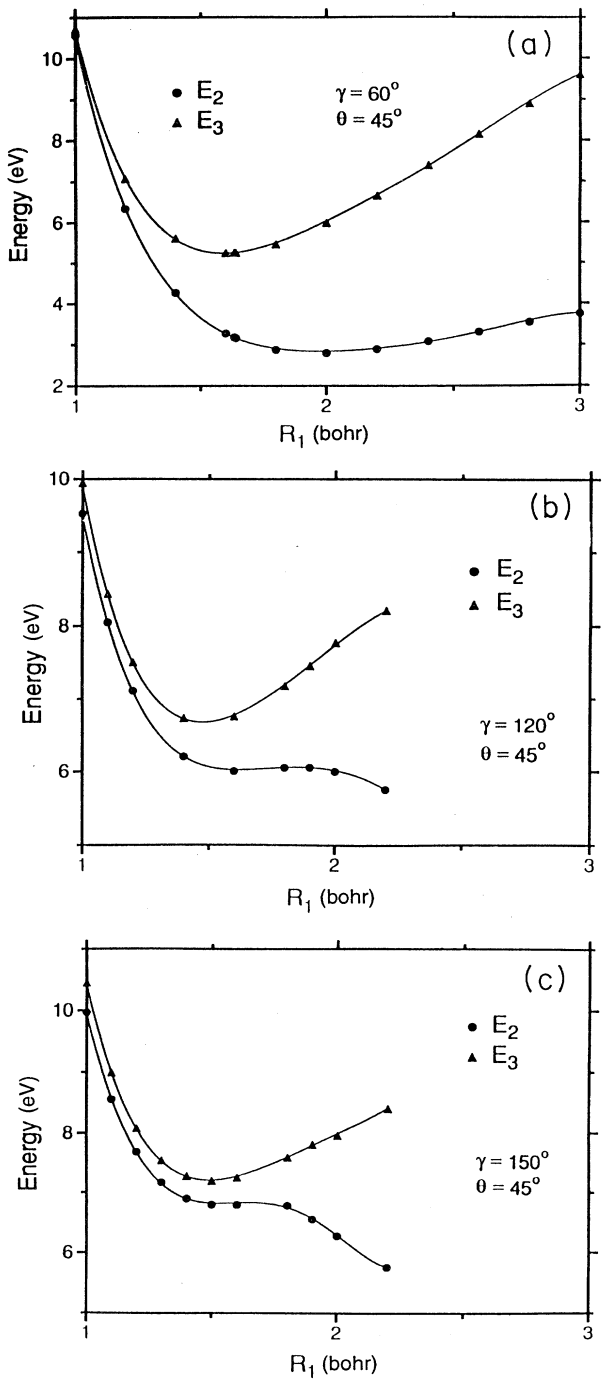

FIG. 10. Potential-energy curves for the E_2 and E_3 states with $\theta=45°$. The energy origin is that of Fig. 4.

to those displayed for $\gamma=60°$. Since the energies of all states have a weak dependence on γ when θ is close to 0° (approaching the separated $H+H_2$ limit), we have restricted ourselves to display the variations of E_2 and E_3 with γ for the single value $\theta=45°$ [see Figs. 10(a)–10(c)]. Again an avoided crossing in E_2 around $R_1=R_2=1.8$ bohrs is seen for γ in the range of 150° and 180°.

It is obvious that the RMCS surface fitting method is not appropriate to be applied to fit the potential-energy surfaces of E_2 and E_3 because of their rich and complicated features resulting from several avoided crossings. More elaborate methods [134,135] will be necessary for this purpose.

The only electric-dipole transition moment that displays reasonably smooth behavior is T_{41} between the E_1 and E_4 states. Since the transition moment is a combination of two electronic wave functions and a dipole moment operator, it should have more features and variations (see Tables IX–XI). For the rest of the transition moments involving E_2 and E_3, the situation is more complicated. Fortunately, in ordinary applications, these moments are only needed in a very limited range of nuclear configuration. A localized fit to the transition moments will suffice for most practical needs.

The potential energies of the E_1 and E_4 states on cuts of constant γ and θ display a very simple Morse-like behavior. The RMCS surface fitting method has been applied to obtain the RMCS potential-energy surfaces for both states. The results are discussed in the next section.

IV. RMCS SURFACES FOR E_1 AND E_4

The potential-energy surfaces for the lowest state of A_1' symmetry (E_1) and the lowest state of A_2'' symmetry (E_4) display simple functional properties and can be described easily using the RMCS potential-energy surface fitting method [128–130]. In the following, we first discuss the GMF5 fits [131,132] to the *ab initio* energies of E_1 and E_4 along the constant (γ,θ) cuts and the quality of the fits. Then the full three-dimensional RMCS fits to E_1 and E_4 and the quality of the RMCS fits are discussed. At the end, the surface features and topology displayed by the E_1 and E_4 RMCS surfaces are presented.

A. GMF5 fits along the constant (γ,θ) cuts

Since the data points are chosen to be along the cuts of constant (γ,θ), the GMF5 fitting is done in a straightforward manner. The reference energies at the swing point P_s (see Fig. 3) are chosen to be $-1.499\,994$ hartrees for E_1 and $-1.124\,718$ hartrees for E_4 (see Sec. III A). The rms deviation is less than 2.3 meV and the maximum deviation is less than 3.5 meV in the resulting GMF5 fitting of the E_4 energies for all constant (γ,θ) cuts. For E_1, the corresponding values are 2.4 and 4.6 meV.

The Morse parameters $D_e(\gamma,\theta)$ $l_e(\gamma,\theta)$, $\beta_0(\gamma,\theta)$, $\lambda_1(\gamma,\theta)$, and $\lambda_2(\gamma,\theta)$ [see Eqs. (4)–(6)] are the results of the GMF5 fits. For a given γ value, after all ten sets of GMF5 fits are done for $\theta=0°,20°,30°,35°,40°,41°,42°,43°,44°,45°$, the smoothness of these parameters with respect to θ is checked. If the parameters display excessively large fluctuations, we then go back to the GMF5 fitting step and make some adjustments, trying to reduce these fluctuations. After one or two iterations, the resulting Morse parameters become reasonably smooth.

The behaviors of GMF5 parameters (for the E_1 and E_4 surfaces) are similar for different γ values. The first three parameters D_e, l_e, and β_0 are smooth functions of θ while λ_1 and λ_2 still display some rapid fluctuations. Since they are first- and second-order corrections to β_0, their effect in the GMF5 function is minor as long as $|x|=|l-l_e|$ is small [Eqs. (4)–(6)]. For the same reason, they are very sensitive to the locations of the *ab initio* points. The nonphysical fluctuation in λ_1 and λ_2 is reduced by choosing the smoothest curve going through almost all of the error bars if possible. The smoothed GMF5 fits are still in quite good agreement with the *ab initio* data. For all constant $\gamma=55°$, 60°, 65°, 75°, 85°, 90°, 100°, 110°, 120°, 150°, and 180°, the rms deviation of the smoothed GMF5 fit to E_4 is less than 6.6 meV and the one for E_1 is less than 4.4 meV. Indeed this visual smoothing does decrease the accuracy of the GMF5 fits, but since the effect of λ_1 and λ_2 is only prominent in the region further away from the bottom of the GMF5 curve (that is, high potential energies), which is of less chemical interest, this degradation of the fitting quality is not too serious for the practical applications of those surfaces. Because of the conical intersection between E_1 and E_2 in the equilateral triangular configurations, the discontinuity of the first derivatives of those GMF5 parameters at $\theta=45°$ is well justified.

B. Three-dimensional RMCS fits

With this set of smoothed GMF5 parameters known at all nodes of the two-dimensional (γ,θ) mesh, the three-dimensional RMCS potential-energy surfaces for E_1 and E_4 are then coded into FORTRAN subroutines in an easy-to-use form. In the case that two bond angles of H_3 are larger than (or equal to) 60°, there are two ways of obtaining the potential energy from the RMCS surface. The permutation symmetry of identical particles requires those two results to be equal. But the RMCS method does not have this property of the potential surface built in and the two choices of γ and the other two internal coordinate variables might lead to different RMCS energies for lack of self-consistency.

Since we use the maximum bond angle as γ, the resulting surface does have the full P_3 symmetry. The drawback of this scheme is that the fitting accuracy decreases for all cuts with $\gamma=60°$, especially when θ approaches 0°. For example, for a set of *ab initio* points of E_4 along the cut of $\gamma=60°$, $\theta=0°$, the GMF5 fit is very good, with a rms deviation of 0.6 meV and a maximum deviation of 1.6 meV. For a given nuclear geometry configuration on this cut with $R_1=2.0$ bohrs (which corresponds to $R_1=2.0$ bohrs, $R_2=10$ bohrs, and $R_3=9.1652$ bohrs), the three bond angles of the triangle have values of 105.6°, 60°, and 14.4°. Choosing the maximum bond angle one uses $\gamma=109.1066°$, $\theta=5.9576°$, and $l=8.0434$

bohrs instead of $\gamma=60°$, $\theta=0°$, and $l=8.0$ bohrs to evaluate the E_4 RMCS energy. Even though both sets of values describe the same nuclear geometry configuration, the first set leads to a RMCS energy 82.7 meV away from the *ab initio* result while the second set leads to a RMCS energy only less than 1.6 meV away from the *ab initio* value.

This problem can be solved in two ways. The first is to use a coordinate system that implemented the full P_3 identical particle symmetry. This will remove the twofold redundancy and the ambiguity left in our RMCS fitting procedure. The difficulty with this procedure is that our present *ab initio* data might not be located at the best positions in the new coordinates for an easy and good fit. The second is to fine-tune the current RMCS surface fit in order to achieve the self-consistency of the surface. Since the ambiguity occurs in the range $60° \leq \gamma \leq 120°$, in which the Morse parameters change noticeably, it would be desirable to obtain more *ab initio* points.

C. Quality of the RMCS fits

In order to address the quality of the three-dimensional RMCS fits for E_1 and E_4, we did the direct comparison between the energies of RMCS fits and the *ab initio* ones. For the E_1 state, we also did several comparisons between our *ab initio* results and their corresponding RMCS ones with the known SLTH and DMBE surfaces [13,14]. Surface features in some selected nuclear geometries are also presented.

In Table XII we list all results of comparison for E_1. The average difference between the *ab initio* energies and the corresponding SLTH values is 0.051 eV (1.2 kcal/mole), the corresponding rms deviation is 0.064 eV (1.5 kcal/mole), and the maximum deviation is 0.34 eV (7.8 kcal/mole). The closeness between the values of the average difference and that of the rms deviation suggests that the present *ab initio* E_1 surface is more or less parallel to but 0.05 eV above the SLTH surface. The individual energy differences for all 1340 individual nuclear geometries confirm this conclusion with very few exceptions. The average difference between the present *ab initio* energies and the corresponding values of the DMBE surfaces is 0.053 eV (1.2 kcal/mole), the rms deviation is 0.058 eV (1.3 kcal/mole), and the maximum deviation is 0.12 eV (2.8 kcal/mole). This set of data shows that the present *ab initio* results agree better with the DMBE surface than with the SLTH one. It is worth mentioning that when the E_1 RMCS surface is compared with the *ab initio* data, the average difference is 0.19 meV, much smaller than the two previous average values. This is expected to be the case since the RMCS surface is a fit to the set of *ab initio* data.

TABLE XII. Comparisons of the E_1 *ab initio* and RMCS surfaces with the SLTH and DMBE surfaces.

Surfaces	Δ_{av}[a] (eV)	Δ_{rms}[b] (eV)	$\lvert\Delta\rvert_{max}$[c] (eV)
Ab initio and SLTH	0.51[−1]	0.64[−1]	0.34
Ab initio and DMBE	0.53[−1]	0.58[−1]	0.12
Ab initio and RMCS	0.19[−3]	0.20[−1]	0.27
RMCS and SLTH	0.51[−1]	0.67[−1]	0.38
RMCS and DMBE	0.52[−1]	0.61[−1]	0.20

[a]Average value of the difference between the potential-energy surfaces identified in the first column for the 1340 nuclear nuclear configurations at which the *ab initio* surface was calculated. $\Delta_{av} \equiv (1/n)\sum_{(i=1,n)}(x_i - x_{i\ ab\ initio})$, $n=1340$, and x_i stands for E_1 surface data.

[b]Root-mean-square value of the difference defined in footnote a: $\Delta_{rms} \equiv [(1/n)\sum_{(i=1,n)}(x_i - x_{i\ ab\ initio})^2]^{1/2}$.

[c]Maximum of the absolute value of the difference defined in footnote a: $|\Delta|_{max} \equiv \max(1,2,3,\ldots,n)|x_i - x_{i\ ab\ initio}|$.

The comparisons between the RMCS E_1 surface (with the same set of nuclear configurations for which we did the comparison between the *ab initio* surface and the SLTH and DMBE surfaces) with the SLTH and DMBE surfaces show similar trends, with an increase of about 4–5 % in the corresponding rms values.

Since the saddle point of the ground electronic potential-energy surface (E_1) in the collinear nuclear geometry configuration has a very important role in the study of the chemical dynamics of the $H+H_2$ system, we list its location, the barrier height, and the two corresponding force constants in Table VII. The complete definitions of those quantities can be found in Refs. [13] and [14].

All surfaces for the E_1 state have a very similar location for the collinear saddle point, ranging from 1.755 to 1.758 bohrs. The barrier heights of the E_1 RMCS surface and the *ab initio* surface are about 22–25 meV higher than the corresponding DMBE value, or 5–6 % higher. The two force constants for all surfaces agree among themselves quite well. This suggests that these potential-energy surfaces have similar shapes in the vicinity of the saddle point.

We did the GMF5 fit and also the ordinary three-parameter Morse fit to the E_1 *ab initio* data for equilateral triangular configurations. For comparison, the same fits were conducted for the calculated energies at the same set of molecular geometries for the SLTH, DMBE, and RMCS E_1 surfaces. The obtained GMF5 parameters for these four surfaces agree with each other quite well (see Table XIII). The three-parameter Morse fits show the same trends displayed in the GMF5 fits. With only three parameters, this fit is less flexible and the fitting quality is lower than that of GMF5 fit. The three-parameters Morse fit gives a larger well depth D_e, a smaller equilibrium distance R_e, and a larger exponent β_0.

Since there has been no previous work that provides a detailed calculation of the E_4 state, we only did comparison between our RMCS E_4 surface with our 1340 *ab initio* data points, which has yielded $\Delta_{av}=0.64$ meV (14.7 cal/mole) for the average deviation, $\Delta_{rms}=0.021$ eV (0.482 kcal/mol) for the rms deviation, and $|\Delta|_{max}=0.27$ eV (6.16 kcal/mol) for the maximum deviation (see the same definitions in footnotes a, b, and c of Table XII for E_1). The maximum deviation occurs at the point of

molecular configuration with $\gamma=55°$, $\theta=0°$, and $R_1=1.0$ bohr. For such a small R_1, the E_4 state has a high energy and also changes steeply with R_1. The RMCS fit is not flexible enough to fit this point well.

The dominant feature of the E_4 surface is the deep well in equilateral triangular energy configurations. The same GMF5 parameters for the equilateral triangular

TABLE XIII. Fits of the $E_{1,2}$ potential-energy surfaces for equilateral triangular configuration for (a) GMF5 parameters and (b) Morse parameters.

Property	SLTH[b]	DMBE[c]	RMCS[d]	*Ab initio*[e]
	(a) GMF5 parameters[a]			
D_e (eV)	1.992	2.000	1.962	1.962
E_e (eV)[f]	2.756	2.748	2.747	2.747
R_e (bohrs)	1.976	1.969	1.973	1.973
β_0 (bohrs^{-1})	0.726	0.732	0.772	0.772
λ_1 (bohrs^{-1})	0.036	0.027	−0.045	−0.045
λ_2 (bohrs^{-2})	0.022	0.028	0.046	0.049
	(b) Morse parameters[g]			
D_e (eV)	2.030	2.039	1.976	1.978
R_e (bohrs)	1.932	1.924	1.935	1.932
β_0 (bohrs^{-1})	0.825	0.831	0.822	0.828

[a]See the text [Eqs. (4)–(6)] for the definitions of the GMF5 parameters. The minimum of the $E_1(R_1)$ curve is at $R_1=R_e$, listed in (a); the minimum of the model curve V is at $l=l_e$ in Eqs. (4)–(6) and an easy derivation with the help of Fig. 3 yields the relationship $R_e=10.0$ bohrs $-l_e/\sqrt{2}$. By definition [see Eqs. (4)–(6)], l_e is a Morse parameter and R_e is not. However, R_e shows the location of the minimum better, so we list it instead of the equivalent l_e. $E_{1,2}$ means that here, at equilateral triangular configuration ($\gamma=60°, \theta=45°$), $E_1=E_2$.

[b]The fit used the SLTH energies [13] at the same set of nuclear configurations as in the GMF5 fit of the *ab initio* data. The reference energy is the theoretical value of three isolated H atoms. The values of D_e and R_e for the SLTH surface (not obtained from a Morse function) are 1.992 eV and 1.981 bohrs [13].

[c]See footnote b for the selection of the nuclear configurations and the choice of reference energy. The values of D_e and R_e for the DMBE surface [14] (not obtained from a Morse function) are 2.000 eV and 1.973 bohrs [14].

[d]See footnote b for the selection of the nuclear geometry configurations. The reference energy is chosen to be three times the value of the present SCF H(1*s*) energy with the 12*s*4*p*1*d*/7*s*4*p*1*d* basis (see Tables I and II), which is about 0.2 meV above the theoretical value.

[e]The reference energy is the same defined in footnote d.

[f]The energy of the minimum point with respect to that of a separated H+H_2 configuration. It is not one of the GMF5 parameters and has been listed in Table VI. For the SLTH and DMBE surfaces, the accurate H+H_2 energy [133] is used as the reference. For the E_1 RMCS and the *ab initio* surfaces, the energy at the nuclear configuration with $R_1=1.402$ bohrs, $R_2=10$ bohrs, and $R_3=R_1+R_2=11.402$ bohrs is used instead. The difference between the second and the first of these reference energies is 0.040 eV.

[g]Equations (4)–(6) become the three-parameter Morse curve with the restrictions $\lambda_1=\lambda_2=0$ in (b).

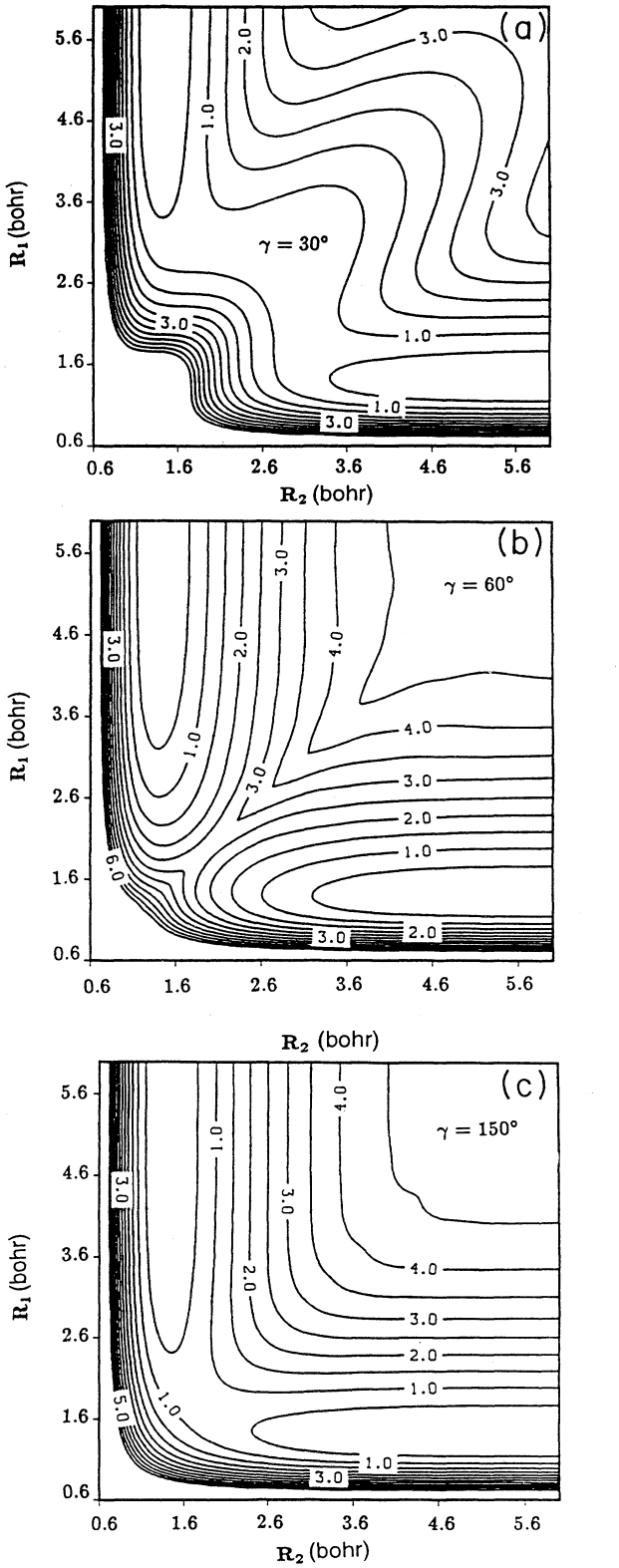

FIG. 11. Two-dimensional equipotential contour plots of the RMCS E_1 potential-energy surface for a given bond angle γ. The contour energies are in the range 0.5–6.0 eV with increments of 0.5 eV. All contour plots have an outermost contour with an energy of 6.0 eV and an innermost one of 0.5 eV. The energy origin is that of Fig. 4.

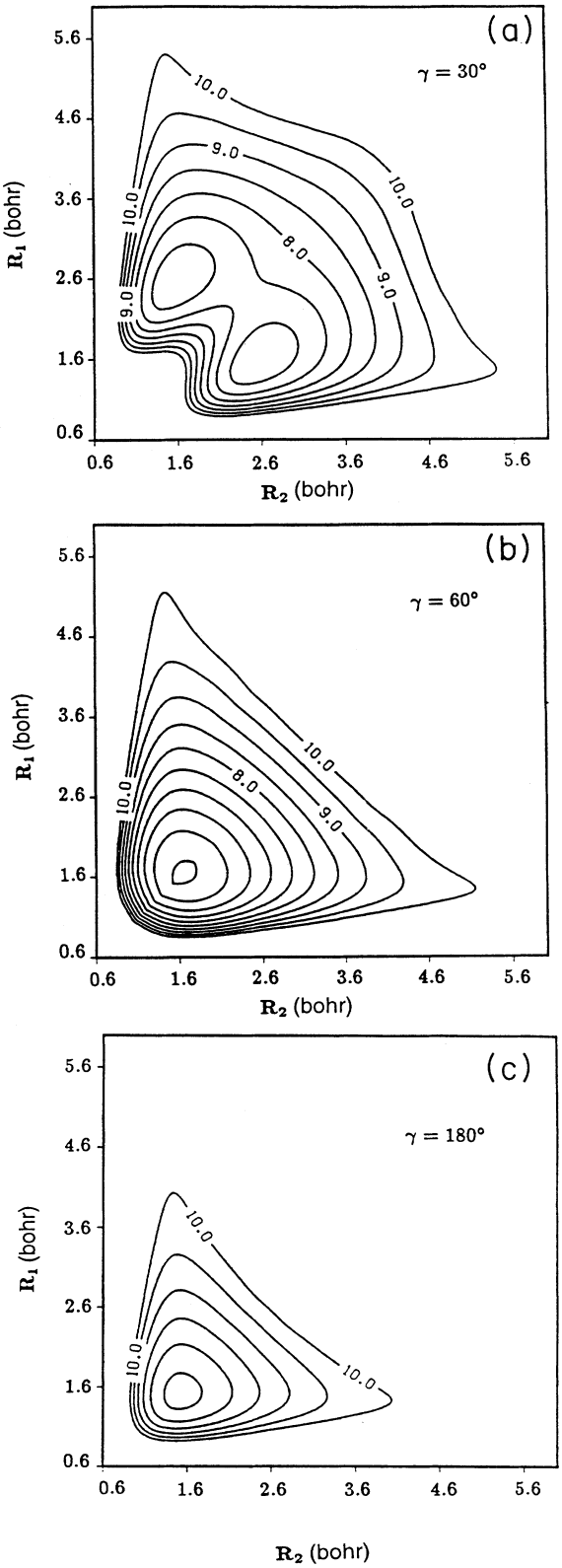

FIG. 12. Two-dimensional equipotential contour plots of the RMCS E_4 potential-energy surface for a given bond angle γ. All contour plots have an outermost contour with an energy of 10.0 eV. The energy step used for all plots is 0.5 eV. The energy origin is that of Fig. 4.

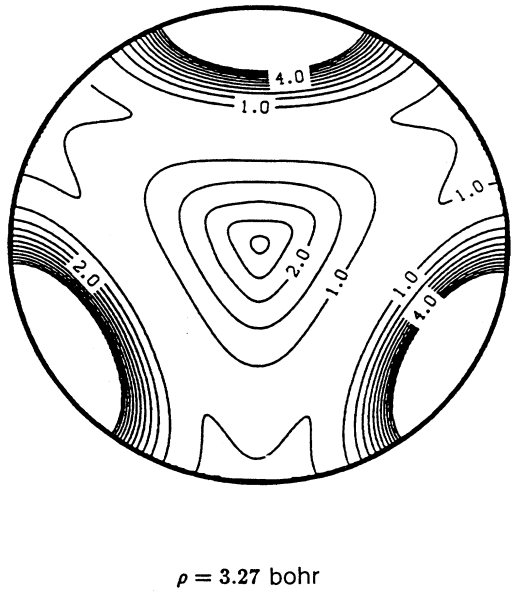

FIG. 13. Equatorial view of the RMCS E_1 potential-energy surface. The hypersphere radius ρ is 3.27 bohrs. The contour energies are in the range 1.0–6.0 eV with increments of 0.5 eV. The center of the plot (a local maximum) corresponds to the lowest conical intersection point of E_1 and E_2. The energy origin is that of Fig. 4.

TABLE XIV. Fits of the E_4 potential-energy surface for equilateral triangular configuration.

Property	RMCS[b]	*Ab initio*[c]
	(a) GMF5 parameters[a]	
D_e (eV)	9.558	9.558
E_e (eV)[d]	5.362	5.362
R_e (bohrs)	1.642	1.642
β_0 (bohrs^{-1})	0.575	0.575
λ_1 (bohrs^{-1})	0.084	0.084
λ_2 (bohrs^{-2})	0.027	0.043
	(b) Morse parameters[e]	
D_e (eV)	9.623	9.632
R_e (bohrs)	1.658	1.656
β_0 (bohrs^{-1})	0.614	0.623

[a]See the text [Eqs. (4)–(6)] for the definitions of the GMF5 parameters and footnote a of Table XIII.
[b]The reference energy is chosen to be the sum of the present SCF energies of $H(2p_z)+2H(1s)$ with the $12s4p1d/7s4p1d$ basis (see Tables I and II), which is about 0.2 meV above the theoretical value.
[c]The reference energy is the one defined in footnote d.
[d]Energy of the minimum point with respect to that of a separated $H+H_2$ configuration. E_e is not one of the GMF5 parameters (see Table XIII). The energy of the *ab initio* E_1 surface at the nuclear configuration with $R_1=1.402$ bohrs, $R_2=10$ bohrs, and $R_3=R_1+R_2=11.402$ bohrs is used as the reference energy. This is higher than the accurate energy Ref. [133] by 0.040 eV.
[e]Equations (4)–(6) become the three-parameter Morse curve with the restrictions $\lambda_1=\lambda_2=0$ in (b).

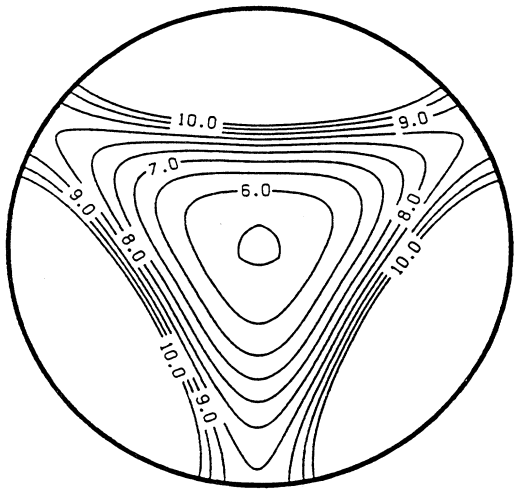

FIG. 14. Equatorial view of the RMCS E_4 potential-energy surface. The hypersphere radius ρ is 2.16 bohrs. The contour energies are in the range 5.5–10.0 eV with increments of 0.5 eV. It shows a deep minimum at the center of the plot, which is the global minimum of E_4. The energy origin is that of Fig. 4.

configuration for the E_4 surface are listed in Table XIV, together with the results of the three-parameter Morse fit. For E_4, three-parameter Morse fit gives larger values of D_e, R_e, and β_0.

D. Contour plots of the RMCS E_1 and E_4 surfaces

The equipotential plots of both RMCS surfaces in the Cartesian coordinates of the bond distances R_1 and R_2 with constant bond angle γ are shown in Figs. 11(a)–11(c) (for the E_1 state) and Figs. 12(a)–12(c) (for the E_4 state). The general features of the RMCS E_1 surface agree well with those of SLTH [13] and DMBE [14] surfaces. The contours of E_1 in Fig. 11(b) ($\gamma=60°$) have a sharp turn for $R_1=R_2$ (or $\theta=45°$) because of the conical intersection between the E_1 and E_2 states. Contour lines with high energy are not as smooth as those with low energy, because the effects of fluctuation of the λ_1 and λ_2 parameters obtained from GMF5 fits are more prominent in the high-energy configuration region. The deep global well of the RMCS E_4 potential-energy surface is clearly depicted in Figs. 12(a)–12(c).

Since the symmetrized hyperspherical coordinates have been very effective in the study of three identical particle system [17–22, 102, 104], we also plot the RMCS E_1 and E_4 surfaces in one of these coordinates [136]. More detailed information is available in Ref. [136]. The equatorial view of E_1 and E_4 on a hypersphere are depicted in Figs. 13 and 14, respectively. The C_{3v} symmetry of the potential-energy surfaces for an identical triatomic system can be seen clearly.

In Fig. 13 the local maximum of the E_1 RMCS surface is located at the center of the plots, which corresponds to an equilateral triangular configuration. The evenly spaced contour lines indicate that it is the conical intersection point between the E_1 and E_2 potential-energy surfaces. In Fig. 14 a local minimum of the E_4 is located at the center of the plots. Three-dimensional color Stardend Application Visualization System (AVS) plots of model potential-energy surfaces E_1 and E_4 are reported in Kristyan's [137] work without the numerical analysis. More numerical data are available in Ref. [127].

V. CONCLUSION

The lowest four electronic states of H_3 have been studied. The results of their energies and corresponding electric-dipole transition moments are obtained. The second and third electronic states display complex behaviors such as avoided crossings, while the first and the fourth ones show a regular rotated-Morse-function-like behavior. The RMCS potential-energy surfaces of both E_1 and E_4 have the right surface features. More studies are needed in order to obtain the potential-energy surfaces of E_2 and E_3.

ACKNOWLEDGMENTS

We acknowledge and thank the U.S. Air Force Astronautics Laboratory (Contract No. F04611-86-0016-67), the Department of Energy (Grant No. DE-A03-83ER), and NSERC (Canada) for financial support. We also thank the NAS program of the NASA–Ames Research Center and the NSF–San Diego Supercomputer Center for use of their CRAY Y-MP systems and the NASA Jet Propulsion Laboratory for use of their CRAY X-MP and Y-MP computers, on which most of the calculations were done. Special thanks are due to Professor R. J. Buenker for supplying us with the CRAY version of the MRD-CI code used in these calculations. Z.P. thanks Dr. Pablo Bruna for assistance.

[1] J. O. Hirschfelder, H. Eyring, and N. Rosen, J. Chem. Phys. **4**, 121 (1936).
[2] R. N. Porter and M. Karplus, J. Chem. Phys. **40**, 1105 (1964).
[3] H. Conroy and B. L. Brunner, J. Chem. Phys. **42**, 4047 (1965).
[4] I. Shavitt, R. M. Stevens, F. L. Minn, and M. Karplus, J. Chem. Phys. **48**, 2700 (1968).
[5] R. N. Porter, R. M. Stevens, and M. Karplus, J. Chem. Phys. **49**, 5163 (1968).
[6] B. Liu, J. Chem. Phys. **58**, 1925 (1973).
[7] P. Siegbahn and B. Liu, J. Chem. Phys. **68**, 2457 (1978).
[8] A. A. Wu, Mol. Phys. **38**, 843 (1979); **42**, 379 (1981).
[9] C. W. Eaker and L. R. Allard, J. Chem. Phys. **74**, 1821 (1981).
[10] M. R. A. Blomberg and B. Liu, J. Chem. Phys. **82**, 1050

(1985).
[11] C. W. Bauschlicher, S. R. Langhoff, and H. Partridge, Chem. Phys. Lett. **170**, 345 (1990).
[12] A. I. Boothroyd, W. J. Keogh, P. G. Martin, and M. R. Peterson, J. Chem. Phys. **95**, 4343 (1991).
[13] D. G. Truhlar and C. J. Horowitz, J. Chem. Phys. **68**, 2466 (1978).
[14] A. J. C. Varandas, F. B. Brown, C. A. Mead, D. G. Truhlar, and N. C. Blais, J. Chem. Phys. **86**, 6258 (1987); Chem. Phys. Lett. **77**, 181 (1981).
[15] G. C. Schatz and A. Kuppermann, J. Chem. Phys. **65**, 4668 (1976).
[16] R. T. Ling and A. Kuppermann, in *Abstracts of the Ninth International Conference on the Physics of Electronic and Atomic Collisions, Seattle, 1975,* edited by J. S. Risley and R. Geballe (University of Washington Press, Seattle, 1975), Vol. 1, pp. 353 and 354.
[17] A. Kuppermann and P. G. Hipes, J. Chem. Phys. **84**, 5962 (1986).
[18] P. G. Hipes and A. Kuppermann, Chem. Phys. Lett. **133**, 1 (1987).
[19] S. A. Cuccaro, P. G. Hipes, and A. Kuppermann, Chem. Phys. Lett. **154**, 155 (1989).
[20] S. A. Cuccaro, P. G. Hipes, and A. Kuppermann, Chem. Phys. Lett. **157**, 440 (1989).
[21] G. A. Parker, R. T. Pack, B. J. Archer, and R. B. Walker, Chem. Phys. Lett. **137**, 564 (1987).
[22] R. T. Pack and G. A. Parker, J. Chem. Phys. **87**, 3888 (1987).
[23] J. Linderberg, S. Padkjaer, Y. Ohrn, and B. Vessal, J. Chem. Phys. **90**, 6254 (1989).
[24] B. Lepetit, J. M. Launay, and M. Le Dourneuf, Chem. Phys. **106**, 103 (1986).
[25] J. M. Launay and M. Le Dourneuf, Chem. Phys. Lett. **163**, 178 (1989).
[26] J. Z. H. Zhang and W. H. Miller, Chem. Phys. Lett. **140**, 329 (1987).
[27] J. Z. H. Zhang and W. H. Miller, Chem. Phys. Lett. **159**, 130 (1989).
[28] G. C. Schatz, Chem. Phys. Lett. **150**, 92 (1988).
[29] J. Z. H. Zhang, D. J. Kouri, K. Haug, D. W. Schwenke, Y. Shima, and D. G. Truhlar, J. Chem. Phys. **88**, 2492 (1988).
[30] M. Mladenovic, M. Zhao, D. G. Truhlar, D. W. Schwenke, Y. Sun, and D. J. Kouri, Chem. Phys. Lett. **146**, 358 (1988); J. Phys. Chem. **92**, 7035 (1988); J. Chem. Phys. **91**, 5302 (1989).
[31] C. H. Yu, D. J. Kouri, M. Zhao, and D. G. Truhlar, Chem. Phys. Lett. **157**, 491 (1989).
[32] D. E. Manopoulos and R. E. Waytt, Chem. Phys. Lett. **159**, 123 (1989).
[33] F. Webster and J. C. Light, J. Chem. Phys. **90**, 300 (1989).
[34] K. Haug, D. W. Schwenke, Y. Shima, D. G. Truhlar, J. Z. H. Zhang, and D. J. Kouri, J. Phys. Chem. **90**, 6757 (1986).
[35] J. Z. H. Zhang, Y. Zhang, D. J. Kouri, B. C. Garrett, K. Haug, D. W. Schwenke, and D. G. Truhlar, Faraday Discuss. Chem. Soc. **84**, 371 (1987).
[36] D. W. Schwenke, K. Haug, D. G. Truhlar, Y. Sun, J. Z. H. Zhang, and D. J. Kouri, J. Phys. Chem. **91**, 6080 (1987).
[37] M. Zhao, D. G. Truhlar, D. W. Schwenke, and D. J. Kouri, J. Phys. Chem. **94**, 7074 (1990).
[38] D. W. Schwenke, K. Haug, M. Zhao, D. G. Truhlar, Y. Sun, J. Z. H. Zhang, and D. J. Kouri, J. Phys. Chem. **92**, 3202 (1988).
[39] M. Zhao, M. Mladenovic, D. G. Truhlar, D. W. Schwenke, Y. Sun, D. J. Kouri, and N. C. Blais, J. Am. Chem. Soc. **111**, 852 (1989).
[40] M. Zhao, D. G. Truhlar, D. J. Kouri, Y. Sun, and D. W. Schwenke, Chem. Phys. Lett. **156**, 281 (1989).
[41] N. C. Blais, M. Zhao, D. G. Truhlar, D. W. Schwenke, and D. J. Kouri, Chem. Phys. Lett. **166**, 11 (1990); **188**, 368(E) (1992).
[42] M. Zhao, D. G. Truhlar, N. C. Blais, D. W. Schwenke, and D. J. Kouri, J. Phys. Chem. **94**, 6696 (1990).
[43] D. C. Chatfield, R. S. Friedman, D. G. Truhlar, B. C. Garrett, and D. W. Schwenke, J. Am. Chem. Soc. **113**, 486 (1991).
[44] D. C. Chatfield, D. G. Truhlar, and D. W. Schwenke, J. Chem. Phys. **94**, 2040 (1991).
[45] P. N. Day and D. G. Truhlar, J. Chem. Phys. **94**, 2045 (1991).
[46] D. C. Chatfield, R. S. Friedman, D. G. Truhlar, and D. W. Schwenke, Faraday Discuss. Chem. Soc. **91**, 289 (1991).
[47] S. L. Mielke, R. S. Friedman, D. G. Truhlar, and D. W. Schwenke, Chem. Phys. Lett. **188**, 359 (1992).
[48] S. L. Mielke, D. G. Truhlar, and D. W. Schwenke, J. Phys. Chem. **98**, 1053 (1994).
[49] S. L. Mielke, G. C. Lynch, D. G. Truhlar, and D. W. Schwenke, J. Phys. Chem. **98**, 8000 (1994).
[50] F. M. Devienne and J. C. Rousteau, Acad. Sci. Paris **263B**, 1389 (1966); **267B**, 1279 (1968); **268B**, 1303 (1969).
[51] T. Nagasaki, H. Doi, K. Wada, K. Higashi, and F. Fukuzawa, Phys. Lett. **38A**, 381 (1972).
[52] N. V. Castro de Faria, M. J. Gaillard, J. C. Poizat, and J. Remillieuz, Ann. Isr. Phys. Soc. **4**, 134 (1981).
[53] C. Cisneros, I. Alverez, G. R. Garcia, C. F. Burnett, J. A. Ray, and A. Russek, Phys. Rev. A **19**, 631 (1979).
[54] M. Vogler, Phys. Rev. A **19**, 1 (1979).
[55] J. K. G. Watson, Phys. Rev. A **22**, 2279 (1980).
[56] P. M. Curtis, B. W. Williams, and R. F. Porter, Chem. Phys. Lett. **65**, 296 (1979).
[57] H. Herzberg, J. Chem. Phys. **70**, 4806 (1979).
[58] I. Dabrowski and G. Herzberg, Can. J. Phys. **58**, 1238 (1980).
[59] G. Herzberg and J. G. K. Watson, Can. J. Phys. **58**, 1250 (1980).
[60] G. Herzberg, H. Lew, J. J. Sloan, and J. K. G. Watson, Can. J. Phys. **59**, 428 (1981).
[61] G. Herzberg, J. T. Hougen, and J. K. G. Watson, Can. J. Phys. **60**, 1261 (1982).
[62] G. I. Gellene and R. F. Porter, J. Chem. Phys. **79**, 5975 (1983).
[63] J. F. Garvey and A. Kuppermann, Chem. Phys. Lett. **107**, 491 (1984).
[64] J. F. Garvey and A. Kuppermann, J. Chem. Phys. **86**, 6766 (1987); **88**, 5985 (1988).
[65] S. J. Jeon, A. B. Raksit, G. I. Gellen, and R. F. Porter, J. Chem. Phys. **82**, 4916 (1985).
[66] H. Helm, Phys. Rev. Lett. **56**, 42 (1986); **61**, 298 (1988).
[67] H. Helm, Phys. Rev. A **38**, 3425 (1988).
[68] H. Helm, L. J. Lembo, P. C. Cosby, and D. L. Huestis, in *Fundamentals of Laser Interactions,* edited by X. Ehlotzky (Springer-Verlag, Berlin, 1989), pp. 264–289.
[69] A. Dodhy, W. Ketterle, H. P. Messmer, and H. Walther, Chem. Phys. Lett. **151**, 133 (1988).
[70] S. F. Selgren and G. I. Gellene, Chem. Phys. Lett. **146**, 485

(1988).
[71] H. Figger, M. N. Dixit, R. Maier, W. Schrepp, H. Walther, I. R. Peterkin, and J. G. K. Watson, Phys. Rev. Lett. **52**, 906 (1984).
[72] H. Figger, Y. Fukuda, W. Ketterle, and H. Walther, Can. J. Phys. **62**, 1274 (1984).
[73] A. B. Raksit, R. F. Porter, W. P. Garver, and J. J. Leventhal, Phys. Rev. Lett. **55**, 378 (1985).
[74] W. Ketterle, H. P. Messmer, and H. Walther, Europhys. Lett. **8**, 333 (1989).
[75] W. Ketterle, Chem. Phys. Lett. **160**, 139 (1989).
[76] C. Bordas, P. C. Cosby, and H. Helm, J. Chem. Phys. **93**, 6303 (1990).
[77] N. Bjerre, I. Hazell, and D. C. Lorents, Chem. Phys. Lett. **181**, 301 (1991).
[78] D. G. Truhlar and R. E. Wyatt, Adv. Chem. Phys. **36**, 141 (1977).
[79] G. Herzberg, Annu. Rev. Phys. Chem. **38**, 27 (1987).
[80] J. K. G. Watson, in *From Atoms to Polymers, Isoelectronic Analogies,* edited by J. F. Liebman and A. Greenberg (VCH, Weinheim, 1989), pp. 129–165.
[81] G. I. Gellene and R. F. Porter, Acc. Chem. Res. **23**, 141 (1990).
[82] H. F. King and K. Morokuma, J. Chem. Phys. **71**, 3213 (1979).
[83] M. Jungen, J. Chem. Phys. **71**, 3540 (1979).
[84] R. L. Martin, J. Chem. Phys. **71**, 3541 (1979).
[85] K. C. Kulander and M. F. Guest, J. Phys. B **12**, L501 (1979).
[86] Ch. Nager and M. Jungen, Chem. Phys. **70**, 189 (1982).
[87] S. Raynor and D. R. Herschbach, J. Phys. Chem. **86**, 3592 (1982).
[88] H. J. Foth, H. R. Mayne, R. A. Poirier, J. C. Polanyi, and H. H. Teller, Laser Chem. **2**, 229 (1983).
[89] H. R. Mayne, R. A. Poirier, and J. C. Polanyi, J. Chem. Phys. **80**, 4025 (1984).
[90] H. R. Mayne, J. C. Polanyi, N. Sathyamurthy, and S. Raynor, J. Phys. Chem. **88**, 4064 (1984).
[91] A. C. Roach and P. J. Kuntz, J. Chem. Phys. **84**, 822 (1986).
[92] I. Petsalakis, J. Theodorakopoulos, and J. S. Wright, J. Chem. Phys. **89**, 6850 (1988).
[93] G. H. F. Diercksen, W. Duch, and J. Karwowski, Chem. Phys. Lett. **168**, 69 (1990).
[94] Z. Peng, A. Kuppermann, and J. S. Wright, Chem. Phys. Lett. **175**, 242 (1990).
[95] M. V. Berry, Proc. R. Soc. London Ser. A **392**, 45 (1984).
[96] C. A. Mead and D. G. Truhlar, J. Chem. Phys. **49**, 23 (1979).
[97] C. A. Mead, Chem. Phys. **49**, 23 (1980).
[98] H. C. Longguet-Higgins, U. Opik, M. H. L. Pryce, and R. A. Sack, Proc. R. Soc. London Ser. A **244**, 1 (1958).
[99] G. Herzberg and H. C. Longguet-Higgins, Discuss. Faraday Soc. **35**, 77 (1963).
[100] H. C. Longguet-Higgins, Adv. Spectrosc. **2**, 429 (1961).
[101] C. A. Mead, Chem. Phys. **49**, 23 (1980).
[102] B. Lepetit, Z. Peng, and A. Kuppermann, Chem. Phys. Lett. **166**, 572 (1990).
[103] C. A. Mead, J. Chem. Phys. **72**, 3839 (1980).
[104] B. Lepetit and A. Kuppermann, Chem. Phys. Lett. **166**, 581 (1990).
[105] N. C. Blais, D. G. Truhlar, and C. A. Mead, J. Chem. Phys. **89**, 6204 (1988).
[106] G. Herzberg, *Spectra of Diatomic Molecules,* 2nd ed. (Van Nostrand, Princeton, 1950).
[107] G. Herzberg, *Electronic Spectra and Electronic Structure of Polyatomic Molecules,* 2nd ed. (Van Nostrand, Princeton, 1950).
[108] H. J. Foth, J. C. Polanyi, and H. H. Teller, J. Phys. Chem. **86**, 5027 (1982).
[109] P. R. Brooks, Chem. Rev. **88**, 407 (1988).
[110] A. B. Raksit, R. F. Porter, W. P. Garver, and J. J. Leventhal, Phys. Rev. Lett. **55**, 378 (1985).
[111] B. A. Collings, J. C. Polanyi, M. A. Stolow, and J. W. Tarr, Phys. Rev. Lett. **59**, 2551 (1987).
[112] V. Engel, Z. Bacic, R. Schinke, and M. Shapiro, J. Chem. Phys. **82**, 4844 (1985).
[113] V. Engel and R. Schinke, Chem. Phys. Lett. **122**, 103 (1985).
[114] P. M. Agrawal, V. Mohan, and N. Sathyamurthy, Chem. Phys. Lett. **114**, 343 (1985).
[115] J. L. Krause and M. Shapiro, J. Chem. Phys. **90**, 6401 (1989).
[116] T. Seideman and M. Shapiro, J. Chem. Phys. **92**, 2328 (1990).
[117] T. Seideman and M. Shapiro, J. Chem. Phys. **88**, 5525 (1988), and references therein.
[118] T. Seideman, J. L. Krause, and M. Shapiro, Chem. Phys. Lett. **173**, 169 (1990), and references therein.
[119] D. Talbi and R. P. Saxon, J. Chem. Phys. **89**, 2235 (1988).
[120] The program HONDO can be obtained from the Quantum Chemistry Program Exchange. In the MRD-CI package, it has been solely used in the integral evaluation step.
[121] R. J. Buenker and S. D. Peyerimhoff, Theor. Chim. Acta **35**, 33 (1974).
[122] R. J. Buenker, S. D. Peyerimhoff, and W. Butscher, Mol. Phys. **35**, 771 (1978).
[123] R. J. Buenker, in *Molecular Physics and Quantum Chemistry into the 80s,* edited by P. G. Burton (University of Wollongong Press, Wollongong, 1980).
[124] R. J. Buenker, in *Studies in Physical and Theoretical Chemistry,* edited by R. Carbo (Elsevier Scientific, Amsterdam, 1982) Vol. 21, p. 17.
[125] R. J. Buenker and R. A. Phillips, J. Mol. Struct. THEOCHEM **123**, 291 (1985).
[126] S. H. Lin, B. Fain, and N. Hamer, Adv. Chem. Phys. **79**, 133 (1990).
[127] Z. Peng, Ph.D. thesis, California Institute of Technology, 1990 (unpublished).
[128] J. M. Bowman and A. Kuppermann, Chem. Phys. Lett. **34**, 523 (1975).
[129] J. N. L. Connor, W. Jakubetz, and J. Manz, Mol. Phys. **29**, 347 (1975).
[130] J. S. Wright and S. K. Gray, J. Chem. Phys. **69**, 67 (1978).
[131] P. J. Kuntz and A. C. Roach, J. Chem. Soc. Faraday Trans. II **68**, 259 (1972).
[132] J. S. Wright, J. Chem. Soc. Faraday Trans. II **84**, 219 (1988).
[133] W. Kolos and L. Wolniewicz, J. Chem. Phys. **43**, 2429 (1965).
[134] S. Thareja and N. Sathyamurthy, J. Chem. Soc. Faraday Trans. II **81**, 717 (1985).
[135] S. Chapman, M. Dupuis, and S. Green, Chem. Phys. **78**, 93 (1983).
[136] A. Kuppermann, Chem. Phys. Lett. **32**, 374 (1975).
[137] S. Kristyan, Comput. Phys. **8**, 556 (1994).